GEOTHERMAL AND GROUND WATER EXPLORATION

ON MAUI, HAWAII,

BY APPLYING D.C. ELECTRICAL SOUNDINGS

A THESIS SUBMITTED TO THE GRADUATE DIVISION OF THE
UNIVERSITY OF HAWAII IN PARTIAL FULFILLMENT
OF THE REQUIREMENTS FOR THE DEGREE OF

MASTER OF SCIENCE

GEOLOGY AND GEOPHYSICS

AUGUST 1981

By

Mark D. Mattice

Thesis Committee:

Barry R. Lienert, Chairman
Charles E. Helsley
Dallas B. Jackson
Ralph Moberly

ACKNOWLEDGEMENTS

ABSTRACT

Twenty-one Schlumberger resistivity soundings were performed on the
island of Maui. Analysis consisted of one-dimensional modeling using an
automatic ridge-regression inversion algorithm (Anderson, 1979). The
inversion results were compared with available well-log information and
geologic maps in order to make geologic interpretations.

The soundings were conducted primarily to estimate the depth to and
the electrical resistivity of, seawater-saturated basalt for different
parts of the island. The resistivity of seawater-saturated basalt on
Maui ranges between 3.5 and 60 ohm-meters. The lowest values occurred
near Ukumehame canyon, on the south rift zone of West Maui. In this
area, which is the site of a warm water (33°C) well, the computed
resistivity for seawater-saturated basalt is about 4 ohm-m. Using
typical Hawaiian basalt porosity values of 15% to 25%, Archie's Law
implies temperatures of between 62° and 171°C at depths below 200 meters
in the Ukumehame area.

Freshwater piezometric heads were estimated from the sounding data.
The largest freshwater head (91 m) was obtained in Keanae valley. The
inferred large volume of freshwater is perched on Keanae alluvial
valley fill and is observed in a well (W100) towards the back of the
valley. All other freshwater heads are under 4 m, indicating that the
freshwater lens is rather thin near the coast at the areas surveyed.

TABLE OF CONTENTS

TABLE OF CONTENTS (continued)

LIST OF TABLES

LIST OF ILLUSTRATIONS

LIST OF ILLUSTRATIONS (continued)

I. INTRODUCTION

Groundwater exploration using the direct current electrical method has enjoyed prospering success in Europe, Russia, Japan, New Zealand, India, mainland United States and Hawaii. On the island of Maui two previous studies by J. H. Swartz (1940) and W. M. Adams et al. (1968) have shown excellent determination of the boundary between freshwater-saturated rocks and seawater-saturated rocks. Determining depths to the seawater boundary by the D.C.-resistivity method and utilizing the Ghyben-Herzberg buoyancy relation produced accurate estimates of the static piezometric head in the areas of both studies. The head estimates were confirmed by nearby well observations.

Extending the D.C.-resistivity technique to explore for anomalous subsurface temperatures has been the subject of much research during the last 20 years. Results have shown that moderate increases in temperature can decrease resistivities over an order of magnitude (Darknov, 1962). The sensitive dependence of resistivity on temperature has resulted in the widespread use of resistivity methods for geothermal exploration. Presumably, seawater-saturated rock underlies the whole of Maui island. By comparing the resistivity values of the seawater-saturated unit, low resistivity areas which may have geothermal potential can be located.

Previous studies in Hawaii (Swartz, 1937; Hussong, 1967; Zohdy and Jackson, 1969) have implied, in most cases, that the boundary at the top of the freshwater table is not electrically distinct. In this study the top of the water table is taken to be the point at which the pore spaces are 100% filled with water. In Hawaii it is well known (i.e. Macdonald and Abbott, 1970) that a transition zone (vadose zone) going

from unsaturated to completely saturated pore space exists above the water table. This leads to the concept of critical saturation. The critical saturation represents the minimum saturation for which there is a continuous film of water over all the surfaces in a rock. This film provides a good medium in which electric current may flow, which in turn greatly reduces the resistivity of the rock. Increasing the volume of water, beyond the critical saturation, does not significantly decrease the resistivity. Critical saturation levels generally range from 20% to 80% (Keller and Frischtnecht, 1966).

The resistivity of fluid-bearing rocks is highly dependent on the resistivity of the fluid. The resistivity of the fluid is in turn highly dependent on the concentration and nature of dissolved solids. A large range of dissolved solids in freshwater gives a large range of resistivities for freshwater-bearing rocks. The nearly constant salinity of seawater gives a small range of resistivities for seawater-saturated rocks.

The top of the freshwater table is generally not electrically distinct because there is a diffuse zone of partial saturation; whereas the base of the freshwater table is generally well defined because of a large salinity contrast between freshwater and seawater. Since the base of the freshwater lens is better defined than the top, it is the base which provides the most useful target for groundwater exploration. The nearly constant salinity of seawater makes the resistivity of seawater-saturated rocks mainly dependent on porosity and temperature. This makes the resistivity of the seawater-saturated rock unit the most useful target for geothermal exploration.

In September of 1979, twenty-one resistivity soundings, using the Schlumberger electrode configuration, were performed on Maui as part of the Hawaii Institute of Geophysics Direct Heat Regional Assessment Program. Eleven soundings were located between the towns of Honolua and Maalaea on West Maui and ten were located on the isthmus and around Haleakala (Figure 1).
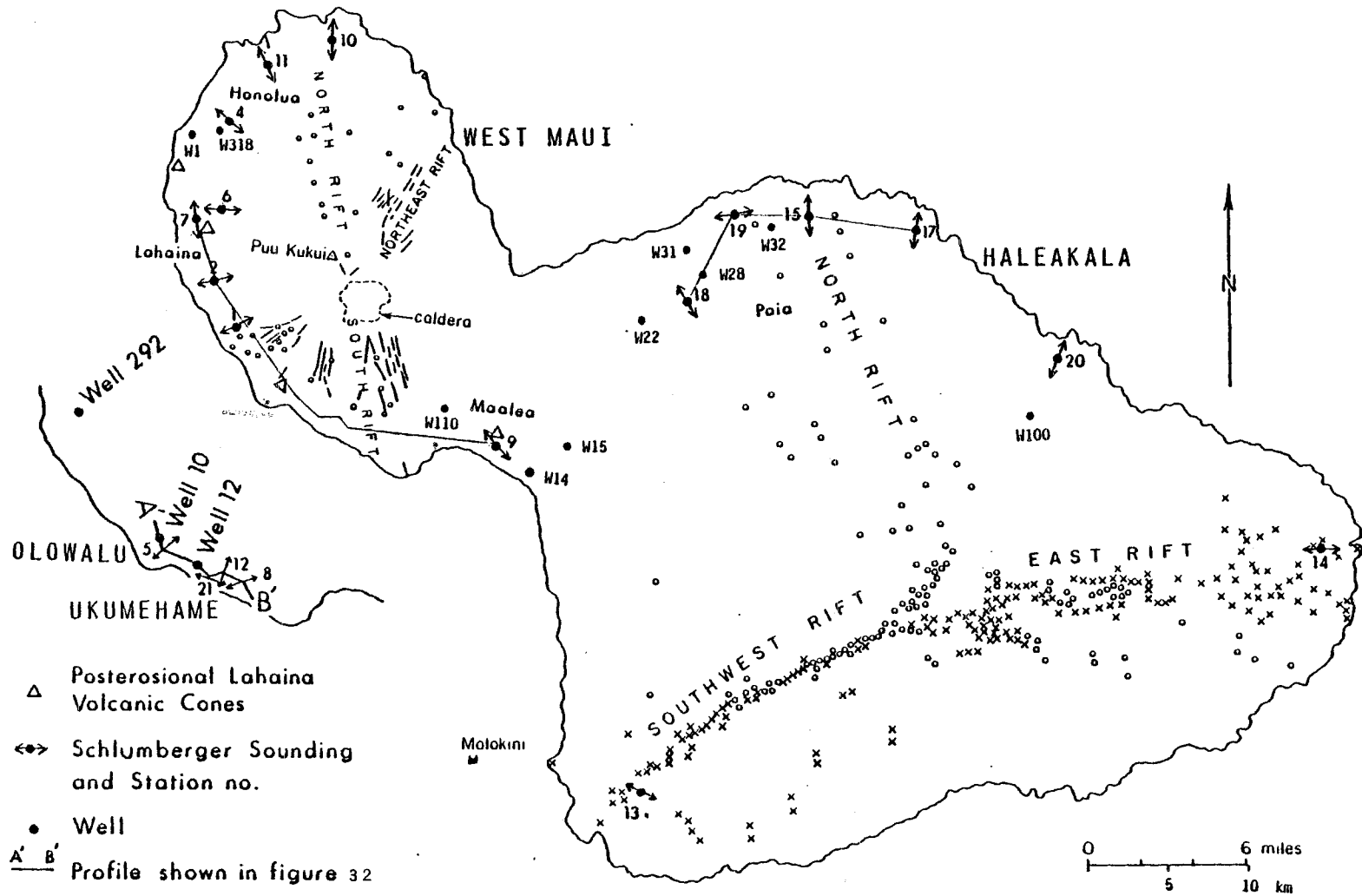
Figure 1. Map of Maui, showing principle volcanic rift zones, dikes (short lines), vents (circles and crosses), wells and Schlumberger sounding locations. (Modified from Macdonald and Abbott, 1970, p. 322 and 331).

II. GEOLOGY OF MAUI

The geology of Maui has been extensively described by Stearns and
Macdonald (1942), then summarized by Macdonald and Abbott (1970). A
summary of Maui's geology and geophysics with regard to geothermal
potential has been given by Thomas et al. (1979).

Maui is the second largest and second youngest island in the
Hawaiian chain. The island is composed of two large volcanoes,
Haleakala and West Maui. Haleakala is considered dormant having last
erupted about 1790. West Maui is considered extinct; its last stage of
activity produced four post-erosional cones in late Pleistocene to Recent
times (Macdonald and Abbott, 1970).

1. WEST MAUI

West Maui consists of three volcanic rock series. The oldest
(Wailuku volcanic series) composing the bulk of the shield is predomi-
nantly thin pahoehoe and aa lava flows of tholeiite, olivine tholeiite,
oceanite and alkalai olivine basalt. The Wailuku basalts are covered
by a thin discontinous andesitic and trachytic lava flows of the Honolua
volcanic series. The last stage of activity, after a long period of
erosion, produced four picritic basalt cones called the Lahaina volcanic
series.

West Maui rift zones are not well defined: dikes radiate in all
directions from the summit. Concentrations of dikes form two general
zones trending southwest to northeast (see Figure 1).

2. HALEAKALA

The main bulk of Haleakala consists of thin-bedded olivine-bearing basalt flows named the Honomanu volcanic series. That shield is almost completely buried by later lavas of the Kula and Hana volcanic series. The Kula series is predominantly hawaiite, alkalic olivine basalt and ankarmite. Rock types of the Hana series are the same as those of Kula series, but the Hana series lava flows erupted after a long period of erosion. Two historic eruptions occurred on the south-west rift zone about 1790 (Macdonald and Abbott, 1970).

Haleakala has three rift zones radial to the caldera complex (Figure 1). The north rift zone has not been active since the long period of erosion. The southwest and east rift zones are predominantly covered with post-erosional Hana series volcanic rocks.

III. REGIONAL GEOPHYSICS OF MAUI

Two regional geophysical surveys have been performed on Maui.
An aeromagnetic survey (Malahoff and Woollard, 1965) was flown at about
3,660 meters elevation. The results of a gravity survey are given by
Kinoshita and Okamura (1965). The surveys deliniate the southwest and
east rift zones of Haleakala as being composed of dense strongly
magnetized material. The north rift zone of Haleakala is well defined
by the gravity survey but not by the aeromagnetic survey. The surveys
indicate that dense strongly magnetized material underlies the caldera
complex of Haleakala.
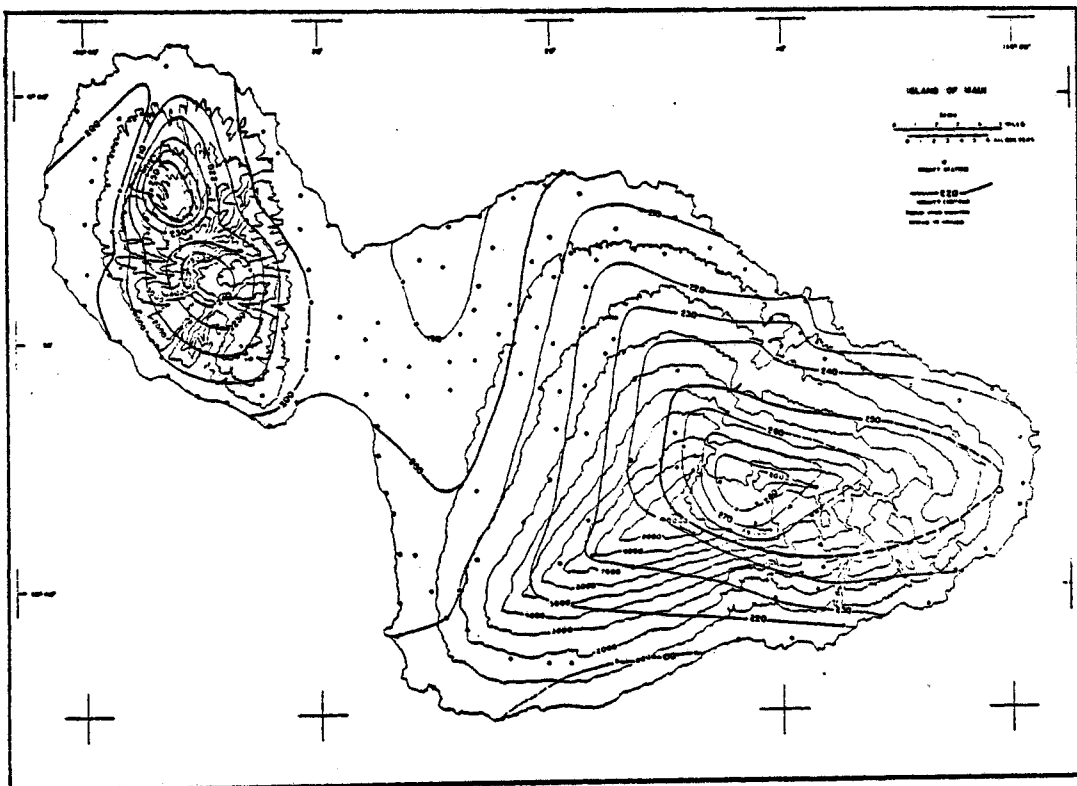
Figure 2. Complete Bouguer anomaly map of the island of Maui, Hawaii
(Reproduced from Kinoshita and Okamura, 1965, p.34)
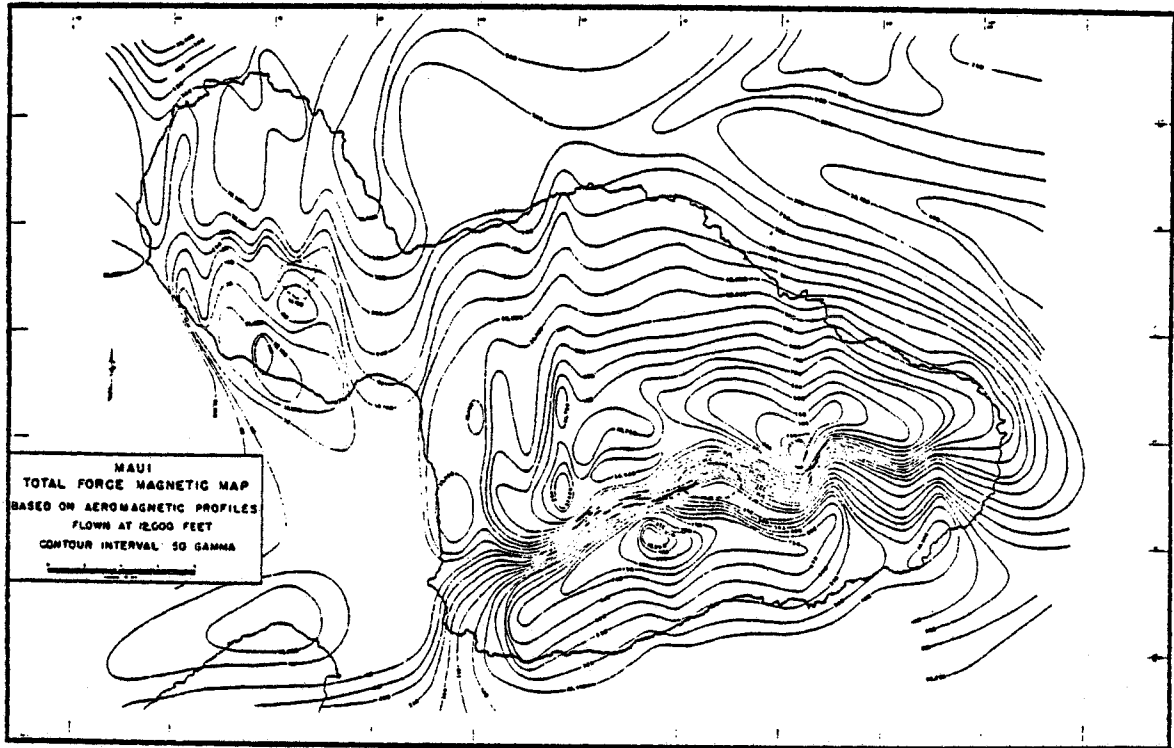
Figure 3.   Aeromagnetic map of the island of Maui, Hawaii.   (Reproduced from Malahoff and Woollard, 1965, p. 19).

The rift zones of West Maui are not delineated in the aeromagnetic survey, but slight elongations in the gravity contours are observed for the north and south rift zones.   The aeromagnetic and gravity data show dense, strongly magnetized material associated with the caldera complex on the southern portion of West Maui.   A second intrusive complex or. pipe zone is indicated in the northern section of West Maui by both gravity and aeromagnetic data.   The aeromagnetic data show a reversely polarized magnetic anomaly near the caldera complex of West Maui.   This may suggest that the magnetic rocks emplaced in the vents near the West Maui caldera occurred during the last reversal epoch.   The last reversed epoch, the Matuyama, occurred between 0.69 and 2.43 million years ago (Cox, 1969).

IV. METHODS AND EQUIPMENT

1. SCHLUMBERGER ARRAY

In the Schlumberger electrical resistivity array, two closely spaced potential electrodes (M and N) are centered in line and between two current electrodes (A and B), as shown in Figure 4.
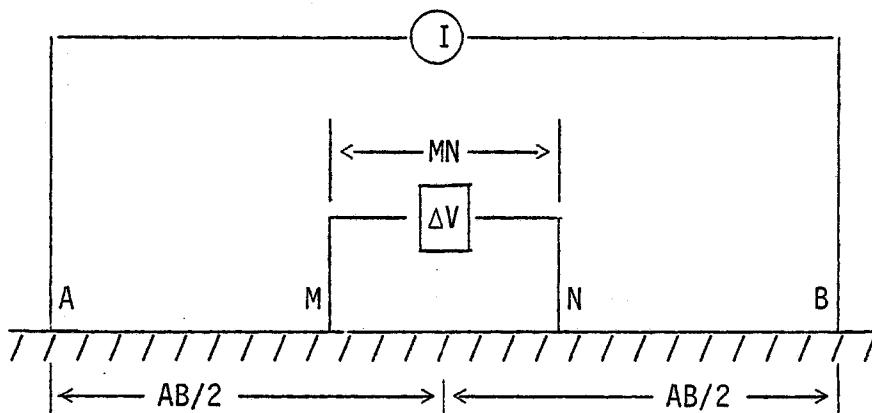
Figure 4. Schlumberger array.

Apparent resistivity in ohm-meters is given by (Keller and Frischknecht, 1966):

$$\rho_a = \frac{\Delta V}{I} \pi \left[\frac{(AB/2)^2}{MN} - \frac{MN}{4} \right]$$ (1)

where ΔV is the measured potential difference in volts, I is the input current in amperes, AB is the current electrode separation and MN is the potential electrode separation. The term in brackets multiplied by pi is the Schlumberger geometric factor. If the earth is composed of a homogeneous and isotropic half-space of resistivity ρ, then $\rho_a = \rho$.

Nonpolarizing copper/copper sulfate porous pots were used as potential electrodes and stainless steel rods as current electrodes. A 1.5 kilowatt portable generator was used for power supply. A Hawaii Institute of Geophysics fabricated current transmitter was capable of providing up to 1 ampere at 1300 volts D.C. Potential differences were measured with a high input impedence (> 10 megohms) Fluke 800A digital multimeter. All connections were made through insulated, multi-stranded copper cables.

Field personnel kept radio contact at all times as a safety precaution. Current leakage was checked periodically to insure that the cables remained properly insulated. Apparent resistivities were plotted bi-logarithmically in the field.

Preliminary interpretations of the sounding data were made by partial curve matching using two-layer master curves (Compagnie Generale de Geophysique, 1955). These initial parameters were used as input for a ridge-regression (modified least-squares) inversion algorithm (Anderson, 1979). The algorithm calculates best-fit resistivity and thickness parameters, their degree of correlation, and standard errors for horizontally layered models.

2. COASTAL CORRECTION

The effect of the low resistivity ocean on soundings performed close to the coastline was estimated using the model of a perfectly conducting, thin semi-infinite sheet, lying on the surface of a homogenous earth (Mundry & Worzyk, 1979). The corrected apparent resistivity, ρ_c, is given by:

$$\rho_c = \frac{\rho_a}{\pi} \left[\tan^{-1}\left(\frac{\sqrt{y+1} + \sqrt{y-1}}{1 - 4y\sqrt{y^2-1}} \right) + \frac{\sqrt{1-1/y}}{2y-1} + \frac{\sqrt{1+1/y}}{2y+1} \right] \qquad (2)$$

for soundings perpendicular to the coast and;

$$\rho_c = \frac{2\rho_a}{\pi} \left[\tan^{-1}(2y) + \frac{2y}{1+4y^2} \right] \qquad (3)$$

for soundings parallel to the coast, where y is the ratio of the distance to the coast from the center of the Schlumberger array to $AB/2$.

All soundings close to the coastline were analyzed at least twice, once with the coastal correction and once without. A good rule of thumb in order to ignore the coastal correction is:

A.) For parallel soundings keep $y \leq 1$. When $y=1$, the error in the apparent resistivity measurement is approximately 4%.

B.) For perpendicular soundings keep $y \leq 2$. When $y=2$, the coastal correction is about 5%.

V. THEORY

1. FUNDAMENTAL EQUATIONS

The fundamental equation for all direct-current resistivity methods is Ohms law, which states:

$$\vec{J} = \frac{\vec{E}}{\rho} \tag{4}$$

where $\vec{E}$ is the electric field in volts/m, ρ is the resistivity of the medium in ohm-m, and $\vec{J}$ is the current density in amperes/m^2. $\vec{J}$ satisfies the divergence theorem, i.e.:

$$\nabla \cdot \vec{J} = 0 \tag{5}$$

which requires that $\vec{J}$ is continuous, i.e. there are no sources or sinks. Combining these two equations and utilizing the relation between electric field and scalar potential,

$$-\nabla V = \vec{E} \tag{6}$$

yields Laplaces equation:

$$\nabla \cdot \vec{J} = 1/\rho \; \nabla \cdot \vec{E} = -1/\rho \; \nabla^2 V = 0 \tag{7}$$

Solutions to Laplaces equation ($\nabla \cdot V^2 = 0$) for a point source of current situated on top of a horizontally layered earth have been given by a number of different authors (e.g. Keller and Frischknecht, 1966). In the Schlumberger array the addition of potentials for two separate

point sources yields a solution. A solution of V which is suitable for computer analysis was given by Stefanesco et al. (1930), and later modified by Slichter (1933). The solution is:

$$V = (\rho_1 \ I/2\pi) \int_0^\infty K_1(\lambda) \ J_0(\lambda r) \ d\lambda \tag{8}$$

where ρ_1 is the resistivity of the surface layer, r is 1/2 the current electrode separation, I is the input current, $J_0(\lambda r)$ is the Bessel function of zero order, λ is the variable of integration with units of reciprocal length and $K_1(\lambda)$ is called Slichters kernel function which depends on the layer parameters. The integral in (8) is called a Hankel transform of order zero.

For a two layer case $K_1(\lambda)$ has the form:

$$K_1(\lambda) = 1 + \frac{2k_1\exp(-2\lambda h_1)}{1-k_1\exp(-2\lambda h_1)} \tag{9}$$

where k is the reflection coefficient:

$$k_1 = \frac{\rho_2 - \rho_1}{\rho_2 + \rho_1} \tag{10}$$

and h_1 is the depth through the first layer. For a 3 layer case the Slichter kernel function is:

$$K_1(\lambda) = 1 + \left[\frac{2(k_1\exp(-2\lambda h_1) + k_2\exp(-2\lambda h_2))}{1 + k_1k_2\exp(-2\lambda(h_2-h_1)) - k_1\exp(-2\lambda h_1 - k_2\exp(-2\lambda h_2)} \right] \tag{11}$$

A recurrence relation for Slichters kernel function has been derived by Pekeris (1940) and is:

$$K_i(\lambda) = \frac{K_{i+1}(\lambda) + (\rho_i/\rho_{i+1})\tanh(\lambda t_i)}{(\rho_i/\rho_{i+1}) + K_{i+1}(\lambda)\tanh(\lambda t_i)} \qquad (12)$$

Note that:

$$\tanh(\lambda t_i) = \frac{\exp(2\lambda t_i) - 1}{\exp(2\lambda t_i) + 1} \qquad (13)$$

where t_i is the thickness of the ith layer.

It is easy to show that Slichters kernel function is equal to 1 for a half-space since V goes to zero as r goes to infinity (Koefed, 1979). Slichters kernel function in the top layer, k_1, can then be obtained by the use of the recurrence relation (12). The potential at the surface of the earth can then be obtained using equation (8).

Multiplying equation (8) by 2 for 2 point sources and differentiating with respect to r, utilizing the relation (Koefed, 1979):

$$\frac{\partial J_0(\lambda r)}{\partial r} = -J_1(\lambda r)\lambda \qquad (14)$$

yields:

$$\frac{\partial V}{\partial r} = -\frac{\rho_1 I}{\pi} \int_0^\infty K_1(\lambda) \, J_1(\lambda r)\lambda d\lambda \qquad (15)$$

where $J_1(\lambda r)$ is the Bessel function of order one. Using the relation,

$$\bar{J} = \frac{I}{\pi r^2} \tag{16}$$

midway between 2 point sources of opposite sign and substituting equation (15) into equation (4) gives:

$$\rho_a(r) = \rho_1 r^2 \int_0^\infty K_1(\lambda) \; J_1(\lambda r)\lambda d\lambda \tag{17}$$

Note that $\rho_a = \rho_1$ for a one-layer model. The integrand in equation (17) may not be a bounded function and the infinite integral may diverge. A suitable rearrangement can be made using Lipschitzs integral:

$$\int_0^\infty \lambda J_1(\lambda r)d\lambda = 1/r^2 \qquad\qquad r > 0 \tag{18}$$

Equation (17) can then be rewritten as:

$$\rho_a(r) = \rho_1 + \rho_1 r^2 \int_0^\infty (\lambda K_1(\lambda) - \lambda) \; J_1(\lambda r)d\lambda \tag{19}$$

where the integrand is now a bounded function and the infinite integral now converges (Koefed, 1979).

2. FORWARD PROBLEM

Inversion of the Schlumberger data was performed by a program written by Walter Anderson (1979) of the United States Geological Survey. A summary of how the program works will be given.

Inversion of Schlumberger data consists of two steps. The first is to calculate the apparent resistivities of a layered model, while the second is to adjust the parameters of the layered model to improve the fit to the field data.

The solution of the forward problem can rapidly be obtained by linear digital filtering. The linear digital filtering technique was first applied to the Schlumberger problem by Ghosh (1971) and improved upon by Koefoed (1972) and Anderson (1975). A good treatment of the subject is given by Koefoed (1979).

Briefly, if the transformations:

$$\lambda = e^{-y} \quad \text{and} \quad r = e^{x}$$

are applied to equation (19) then the apparent resistivity function becomes:

$$\rho_a(r,\vec{p}) = \rho_1 + \rho_1 r \int_0^\infty k_1(e^{-y}) e^{x-y} \, J_1(e^{x-y}) dy \qquad (20)$$

where the vector $\vec{p}$ represents the resistivity and thickness parameters for a given layered model. The integral in equation (20) takes the form of a convolution integral (Anderson, 1975).

$$\rho_a(r,\vec{P}) = \int_{-\infty}^\infty f(y) \, g(x-y) dy \qquad (21)$$

Where $f(y)$ is the input function $\rho_a(r,\vec{p})$ is the output function and the term $g(x-y)$ is called the filter response function. The filter response function can be determined using known input-output Hankel transformation pairs. A value for the apparent resistivity function is obtained as a

sum of products of the sample values of the filter response function with values of Slichters kernel function. The samples are taken at a constant logarithmic interval along the abscissa axis. The coefficients in this linear expression are called the filter weights. The filter weights are only dependent on the sampling interval and can therefore be calculated in advance. The apparent resistivity function is then computed using the equation:

$$\rho(r,\vec{P}) = \rho_1 + \rho_1 r \sum_{i=1}^{NW} W_i \; K_1(\ln r - N_i, \vec{P}) \tag{22}$$

where NW is the number of filter weights, N_i are the absicissa locations of the filter weights, W_i are the filter weights and r is AB/2. Individual points on the resistivity curve are obtained by summing the products of the kernel function with the precomputed suite of filter weights.

3. INVERSE PROBLEM

Resistivity inversion by ridge-regression has been covered by Inman (1975). The major points will be summarized here. The logarithms of apparent resistivity values are used in the inversion which eliminates weighting of individual data values. Application of the Gauss-Newton method (Taylor series expansion) to the problem results in the matrix equation:

$$\Delta G = A \; \Delta P \tag{23}$$

Where ΔG is the vector of differences between the logarithms of the observed apparent resistivities and the logarithms of the apparent resistivities for the current model at each AB/2 spacing. A first-guess model is needed to initiate the program. ΔG has the form:

$$\Delta G = \begin{bmatrix} (\ln\rho_a^o - \ln\rho_a^m)_1 \\ (\ln\rho_a^o - \ln\rho_a^m)_2 \\ \cdot \\ \cdot \\ \cdot \\ (\ln\rho_a^o - \ln\rho_a^m)_n \end{bmatrix} \qquad (24)$$

Where ρ_a^o is the observed apparent resistivity at the nth AB/2 spacing and ρ_a^m is the apparent resistivity of the current model at the nth AB/2 spacing.

ΔP is the difference vector between the logrithmic parameters of the current model and the logrithmic parameters of the unknown model. ΔP has the form:

$$\Delta P = \begin{bmatrix} (\ln\rho_i - \ln\rho_i^m) \\ \vdots \\ (\ln\rho_k - \ln\rho_k^m) \\ (\ln t_{k+1} - \ln t_{k+1}^m) \\ \vdots \\ (\ln t_{2k-1} - \ln t_{2k-1}) \end{bmatrix} \qquad (25)$$

Where ρ_k and ρ_k^m are the kth layer resistivities of the unknown and current model respectively, for a k-layered model.

Matix **A** is the Jacobian matrix, with the form:

$$\mathbf{A} = \begin{bmatrix} \dfrac{\partial G_1}{\partial P_1} & \dfrac{\partial G_1}{\partial P_2} & \cdots & \dfrac{\partial G_1}{\partial P_k} \\[2ex] \dfrac{\partial G_2}{\partial P_1} & \dfrac{\partial G_2}{\partial P_2} & \cdots & \dfrac{\partial G_2}{\partial P_k} \\[2ex] \vdots & & & \vdots \\[2ex] \dfrac{\partial G_n}{\partial P_1} & \cdots\cdots & & \dfrac{\partial G_n}{\partial P_k} \end{bmatrix} \tag{26}$$

Where the element $A_{nk} = \dfrac{\partial G_n}{\partial P_k}$ is the partial derivative of the apparent resistivity at the nth AB/2 spacing with respect to the kth model parameter. The partials can be calculated analytically or numerically. If there are more observations then parameters then matrix **A** is overconstrained. A solution for **Δ P** is then:

$$\mathbf{\Delta P} = (\mathbf{A}^T\mathbf{A})^{-1} \mathbf{A}^T \mathbf{\Delta G} \tag{27}$$

Where **T** represents transpose and -1 means inverse. The matrix $\mathbf{A}^T\mathbf{A}$ often has very small eigenvalues which may make the inverse matrix, $(\mathbf{A}^T\mathbf{A})^{-1}$, unstable.

In such cases, the matrix $\mathbf{A}^T\mathbf{A}$ can be stabilized by adding a constant k to each of its diagonal terms. This leads to a modification of equation (27)(Marquardt, 1963), namely:

$$\Delta P = (A^T A + kI)^{-1} A^T \Delta G \qquad (28)$$

Where I is the identity matrix and k is called the Marquardt factor. By adding a small amount of bias (kI) to the diagonal terms, the inverse matrix becomes more stable.

The Marquardt factor k is large ($k=1.0$) when initiating the program, which allows equation (28) to approach the gradient method (method of steepest decent). The gradient method works well with a poor initial guess (Koefoed, 1979). It may, however, diverge while nearing a solution. The technique then is to let k decrease as the program procedes allowing equation (28) to approach the Gauss-Newton method ($k=0$), which converges rapidly when near a solution. The method of varying k is called ridge-regression. Convergence is complete when ΔP or the sum of squares residual reaches a minimum.

4. ERROR ANALYSIS

The amount of uncertainty is assessed with three statistics, root mean square error due to regression (S), parameter standard deviation (σ_i) and the parameter correlation matrix $\mathbf{COR}(\vec{P})$.

The RMS error (S), due to the departure of the model curve from the field curve, is the objective statistic to be minimized by ridge-regression. The estimate of (S) is given by:

$$S = \left[\frac{1}{n-k+p} \sum_{i=1}^{n} (\rho_a^t - \rho_a^o) \right]^{\frac{1}{2}} \qquad (29)$$

where:

ρ_a^t = theoretical apparent resistivity.

ρ_a^o = observed apparent resistivity.

n = number of data points.

k = number of parameters.

p = number of fixed parameters.

$n-k+p$ = number of degrees of freedom.

Since the inversion is carried out in logarithmic space, where $\Delta \ln\rho_a \simeq \Delta\rho/\rho$, the estimate of percent RMS error is simply:

$$S^1 = \left[\frac{1}{n-k+p} \sum_{i=1}^{n} (\ln\rho_a^t - \ln\rho_a^o)^2 \right]^{\frac{1}{2}} \cdot 100 \qquad (30)$$

The 8000A Fluke digital voltmeter had a specified accuracy of 0.1% of reading + 1 digit. The ampmeter could usually be read with an accuracy of about 2.5% to 5.0%. For small AB/2 and all MN spacings the measurements were very accurate, about 1% or 2% standard deviation. For large AB/2 spacings the estimated standard deviation is about 3%. Using error propagation analysis (Bevington, 1969), and assuming all errors are uncorrelated, an estimate of percent standard deviation for the apparent resistivity calculation is:

$$\frac{\sigma(\rho_a)}{\rho_a} \simeq \left\{ \left(\frac{\sigma(\Delta V)}{\Delta V}\right)^2 + \left(\frac{-\sigma(I)}{I}\right)^2 + \left(\frac{2\sigma(AB/2)}{AB/2}\right)^2 + \left(\frac{-\sigma(MN)}{MN}\right)^2 + \right.$$

(31)

$$\left. \cancel{\left(\frac{\sigma(AB/2)}{K}\right)}^2_{\;0} \left[\frac{KMN}{AB/2} + \frac{MN^2}{16AB/2}\right] + \cancel{\left(\frac{\sigma(MN)}{K}\right)}^2_{\;0} \left[\frac{\pi^2}{4} - \frac{\pi K}{MN}\right] \right\}^{\frac{1}{2}} \cdot 100$$

Where K is the Schlumberger geometric factor. The last two terms on the right hand side go to 0 since K is large compared to the variance in AB/2 and MN.

In the most favorable circumstances, when AB/2 and MN are small, a large amount of current penetrates the ground (>100ma) and large potential differences are measured (>50mv) the estimated standard deviation due to measurement error is about 3%. When the potential difference is small (<1mv) then the measurement errors may be as large as 50%. The potential difference measurement usually has an accuracy better than 4%.

Assuming a 4% standard deviation for the potential difference, a 2.5 to 5.0% error in the current reading, a 1 to 3% error in AB/2 and 1 or 2% error in MN and using equation (31) then the estimated standard deviation for ρ_a is between 5 and 9%. If the value of S, as determined by ridge-regression, is less than or equal to 9% the solution is considered consistant with the field data. Seventy-four percent of the Schlumberger solutions, performed on Maui, were found to be consistent with the field data.

The estimated covariance matrix between parameters is (Jenkins & Watts, 1968):

$$\mathbf{COV}\ (\vec{P}) = S^2 (\mathbf{A}^{\mathsf{T}} \mathbf{A})^{-1} \tag{32}$$

Where **A** is the Jacobian matrix. The estimate of individual parameter standard deviations (σ_i) are the square roots of the diagonal elements of the covariance matrix (Jenkins and Watts, 1968):

$$\sigma_i = \sqrt{\mathbf{COV}\ (P)_{ii}} \tag{33}$$

In order to estimate if σ_i is a good measure of the uncertainty of parameter i the correlation matrix **COR** $(\vec{P})$ is calculated. The correlation matrix is defined as:

$$\mathbf{COR}(P)_{ij} = \frac{\mathbf{COV}(P)_{ij}}{\left[\mathbf{COV}(P)_{ii} \times \mathbf{COV}(P)_{jj}\right]^{\frac{1}{2}}}$$

If the correlations are small then the standard deviation is a good measure of the uncertainty. If the correlation coefficient between 2 parameters is very near unity, then the true uncertainty will be large (usually >100%). The true uncertainty, however, will be overestimated by the standard deviations when the correlation coefficient is near unity (Draper and Smith, 1966). In order to illustrate what is being measured with the correlation coefficient, two sections of solution space are plotted in Figure 5.

uncorrelated parameters   correlated parameters
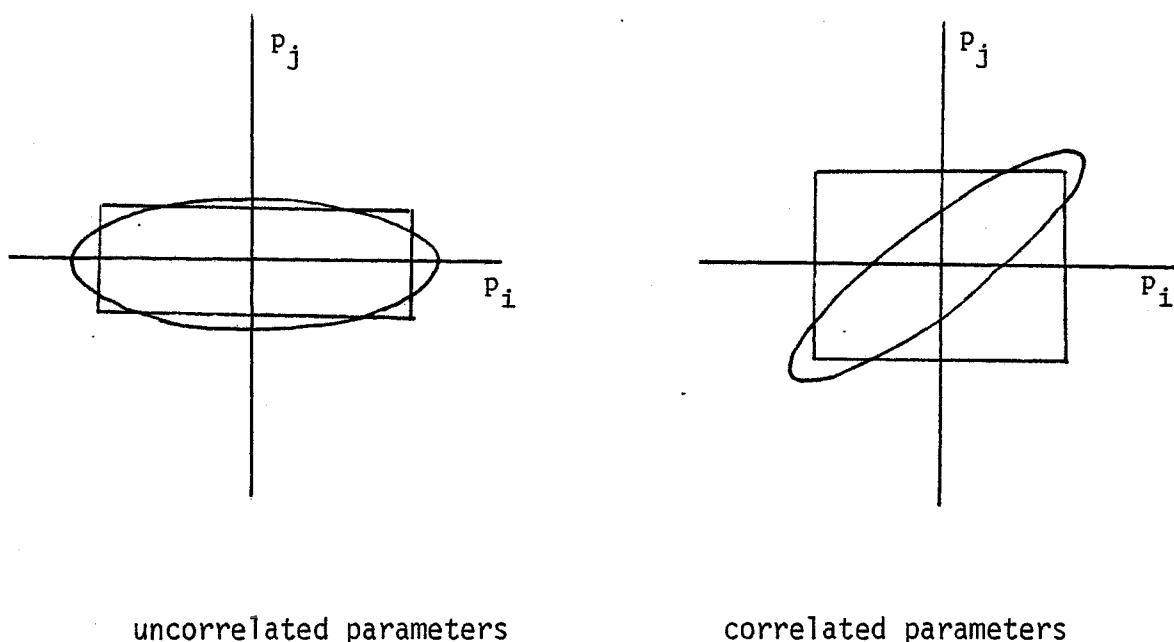
Figure 5. Graphical representation of correlation coefficients.
         (Modified from Draper and Smith, 1966, p. 65-66.)

The origin indicates the 2 parameter values in the final solution, i.e. at the minimum sum of squares. The 2 parameter values may be any combination of parameters (resistivities and thicknesses). The contour encloses the 68% confidence region for the values of P_i and P_j, while the box limits are given by the standard deviations. If the 2 parameters

are uncorrelated then the region indicated by the box is a good estimate of the confidence region. The ellipticity and tilt of the ellipse in Figure 5 is measured by the correlation coefficient. When the correlation is near unity then the errors in the 2 parameters are nearly linearly dependent and the region enclosed by the box overestimates the actual confidence region (Inman, 1975). Use of the box limits do, however, estimate the maximum range of uncertainty in each parameter. When more than two parameters are correlated it is necessary to compute higher dimension confidence regions in order to estimate the uncertainty accurately.

VI. LIMITATIONS

Slichter (1933) proved mathematically that a unique solution, for the direct current method, exists provided that resistivity is a continuous function with depth. For horizontally layered models King (1935) indicates that no unique solution can be obtained from the knowledge of the potential about a point source of current.

For a given number of layers the problem of non-uniqueness results primarily from inadequate measuring accuracy. When the apparent resistivity curve does not asymptotically approach the resistivity of a particular layer then there may exist an equivalent model distribution which gives almost the same apparent resisitivity curve. This problem has been described by the principles of equivalence and suppression.

1. PRINCIPLE OF EQUIVALENCE

The principle of equivalence concerns a layer sandwiched between two or more layers (Maillet, 1947).

A resistive layer between two conductive layers ($\rho_1 < \rho_2 > \rho_3$), has a transverse resistance equal to the product of its resistivity and thickness ($T_2 = \rho_2 t_2$). Two three-layer sections with the same ρ_1, ρ_3 and T_2 may have practically identical sounding curves. This is called equivalence by T and also applies approximately to curves where $\rho_1 > \rho_2 > \rho_3$.

A conductive layer between two resistive layers ($\rho_1 > \rho_2 < \rho_3$), has a horizontal conductance equal to the ratio of its thickness to resistivity ($S_2 = t_2 / \rho_2$). Two three-layer sections with the same ρ_1, ρ_3 and S_2 may have practically identical sounding curves. This is called equivalence by S and also applies to curves where $\rho_1 < \rho_2 < \rho_3$.
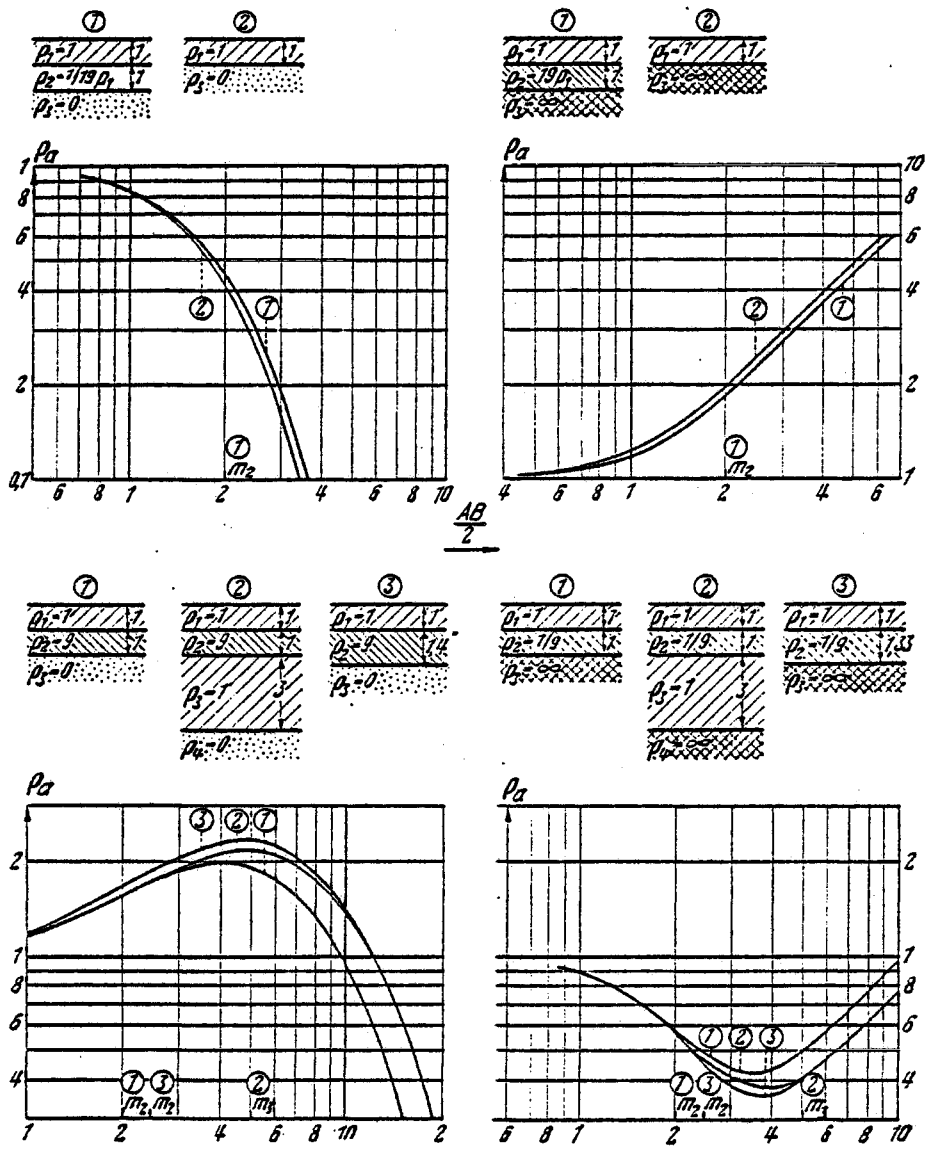
Figure 6. Principle of equivalence and its limits.
(Reproduced from Kunetz, 1966, p.59).

The range of the principle of equivalence depends on the ratios ρ_2/ρ_1 and t_2/t_1. Nomograms published by Keller and Frischknecht (1966) define the range of equivalence. The rules of equivalence have only a restricted validity, since they depend on the whole suite of parameters encountered. If two or more layers show equivalence relations then the concept of an equivalent layer distribution must be considered. This assessment is best undertaken by computing the parameter correlation matrix which was discussed under the section on error analysis. Figure 6 demonstrates the principle of equivalence.

2. PRINCIPLE OF SUPPRESSION

A Schlumberger sounding curve measured over a four-layer earth may be nearly equivalent to one measured over a three-layer earth. This is known as the principle of suppression. Suppressed layers are usually thin with respect to their depth and have a resisitivity intermediate between two enclosing layers; as the thickness increases the influence of a suppressed layer on the resistivity curve becomes more apparent. Four examples of suppressed layers are shown in Figure 7.

The phenomena of equivalence and suppression result primarily from inadequate measurement accuracy. Measurement errors are on the order of 8% (see section on error analysis). Large differences between layer parameters may have an effect on the apparent resistivity curve which is smaller than the 8% measuring error.
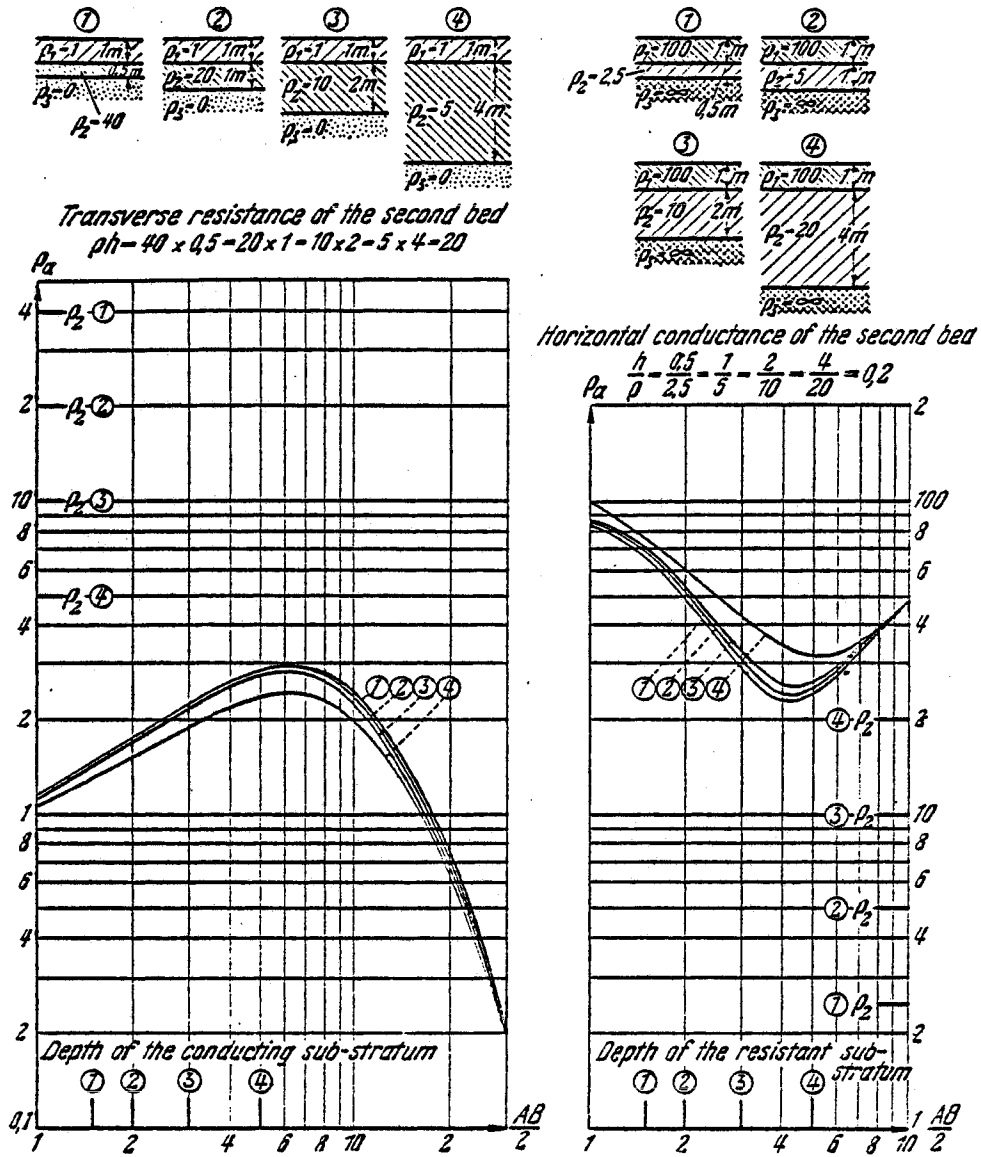
Figure 7. Principle of suppression, h = thickness and
ρ = resistivity. (Reproduced from Kunetz,
1966, p. 60).

3. ANISOTROPY

A fundamental assumption in computing layered resistivity models is that the layers are isotropic, i.e. the resistivity within a particular layer is the same in all directions. Geologic layers may, however, be anisotropic. For example, this could happen in thick layers of basalt. A basaltic unit is usually made up of several thin-bedded lava flows, commonly with clinker zones separating individual flow units. Under these conditions the electrical resistivity may be equal to ρ_ℓ in all horizontal directions, but equal to a different value, ρ_t, in the vertical direction. The ratio ρ_t/ρ_ℓ for all practical purposes seldom excedes 3 (Keller and Frischknecht, 1966).

When a layer is anisotropic the actual resistivity being measured by the Schlumberger technique is the average resistivity ρ_m:

$$\rho_m = \sqrt{\rho_\ell \cdot \rho_t} \tag{34}$$

the actual thickness being measured is t_m:

$$t_m = t\sqrt{\rho_\ell/\rho_t} = t\alpha \tag{35}$$

where α is called the coefficient of anisotropy, and is always greater than or equal to 1, for horizontally layered models.

The effect of anisotropy cannot be determined by the Schlumberger sounding technique. If it is neccessary to evaluate anisotropy then other types of measurements are neccessary, such as resistivity well

logging. The effect of anisotropy, if it exists, is that too large a thickness will be obtained for the anisotropic layer.

4. HETEROGENEITIES

Another assumption in one-dimensional resistivity studies is that the earth is composed of homogenous layers. However geologic layers such as sediments often contain lateral inhomogeneities such as boulders or mineralization deposits. When such heterogeneities are near the surface and near the measuring electrodes, the potential distribution will be distorted (Figure 8). Such local variations can cause large errors in the measured resistivities.

Conductive
Heterogeneity

Resistive
Heterogeneity
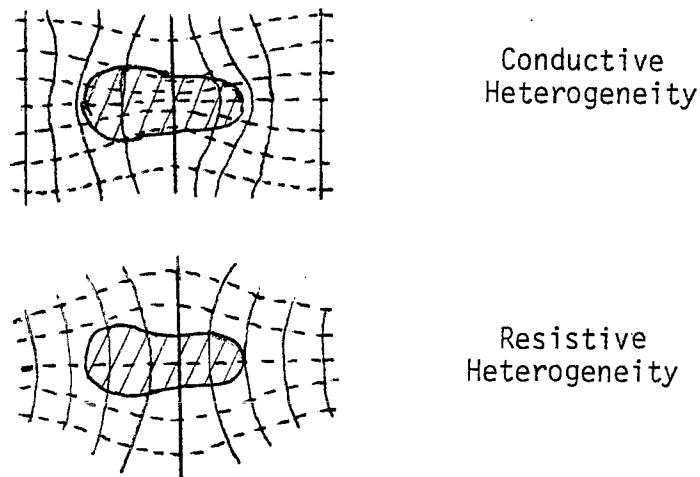
Figure 8. Distortion of potential lines at the earths surface due to local heterogeneities. Solid lines are equipotentials, dotted lines are current lines. (Modified from Kunetz, 1966, p.13).

The effect of a resistive heterogeneity near the potential electrodes is to increase the measured potential difference, this causes an increase in the measured apparent resistivity. For a conductive heterogeneity the opposite is true, giving an apparent resistivity which is too small.

In the Schlumberger array the potential electrodes are held fixed while the current electrodes are expanded to increasingly greater separations. Periodically, the current electrodes are held fixed while the potential electrodes are expanded to a larger interval. In this way the effect of a heterogeneity near a measuring electrode remains constant as the current electrode spacing is increased. As long as the ratio AB/MN is greater than 10 the measured apparent resistivities, at two different MN separations with the same AB separation should be within 4% of each other (Mundry, 1980). If the two resistivities are very different then heterogeneities are probably the cause (Figure 9).

The approach of some investigators when a shift in the apparent resistivity curve is observed, like those shown in Figure 9, is to adjust the offset section up or down to match the rest of the curve (Zohdy et al., 1974). In this manner approximating more closely the true horizontal layering. No published study has proven that this "shifting" is valid. Results of this study indicate that this shifting is a better, but crude, approximation to the true horizontal layering.

5. DEPTH OF INVESTIGATION

Results in section VII show that seawater-saturated basalt is the most useful geologic unit on the island of Maui for the purposes of geothermal and hydrological assessment. In order to maximize the
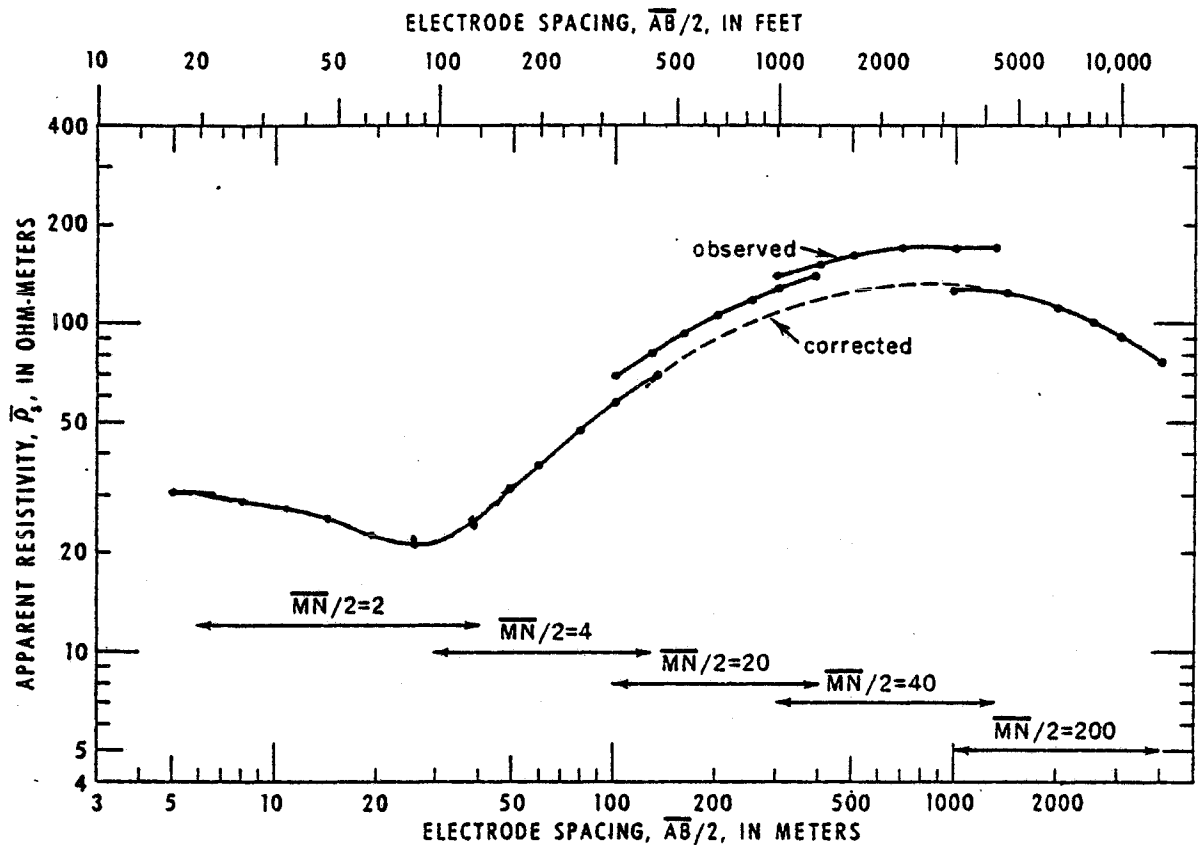
Figure 9. Effect of resistive heterogeneity near potential
electrodes at two MN spacings and method of cor-
rection. (Modified from Zohdy et al, 1974, p.41).

likelihood of resolving depth to and resistivity of the seawater base-
ment several points must be considered. They include depth of

investigation, distance to the coastline, elevation of the sounding

and spread length of the Schlumberger array.

Depth of investigation was first defined by Evjen (1938) for

the Wenner array and later expanded to include the Schlumberger array

by Roy and Apparo (1971). They define the depth of

investigation as the depth where a thin horizontal layer of ground contributes the maximum amount to the total measured signal at the ground surface. For a homogeneous earth the depth of investigation is AB/8. For a two layer earth with a resistivity contrast of less than 3 the depth of investigation remains about the same. In order to resolve the resistivity of the basement in a two layered model a spread length 8 times the thickness of the surface layer is necessary.

The depth of investigation for 2 or more layers largely depends on the contrasts between layer resistivities. A set of two layer curves for the Schlumberger array is reproduced in Figure 10. Each curve varies smoothly and uniformly from an apparent resistivity which is close to the resistivity of the upper layer for the small electrode separation to an apparent resistivity which is close to the half-space resistivity for large electrode spacings. The curves for the cases in which the 2nd layer is more conductive than the surface layer and the resistivity contrast between the two layers is less than 1/3 begin to flatten approximately at AB = 8h, where h is the thickness of the upper layer. When the contrast is large then the depth of investigation decreases. For example, with a contrast of 1/100 the curve does not flatten until AB = 16h. If the basement is more resistive than the surface layer, the depth of investigation is largely dependant on the resistivity contrast. For example when the basement resistivity is 100 times the resistivity of the surface layer then the Schlumberger array would have to be expanded to approximately AB = 50h before the apparent resistivity curve would begin to flatten out to the half-space resistivity.
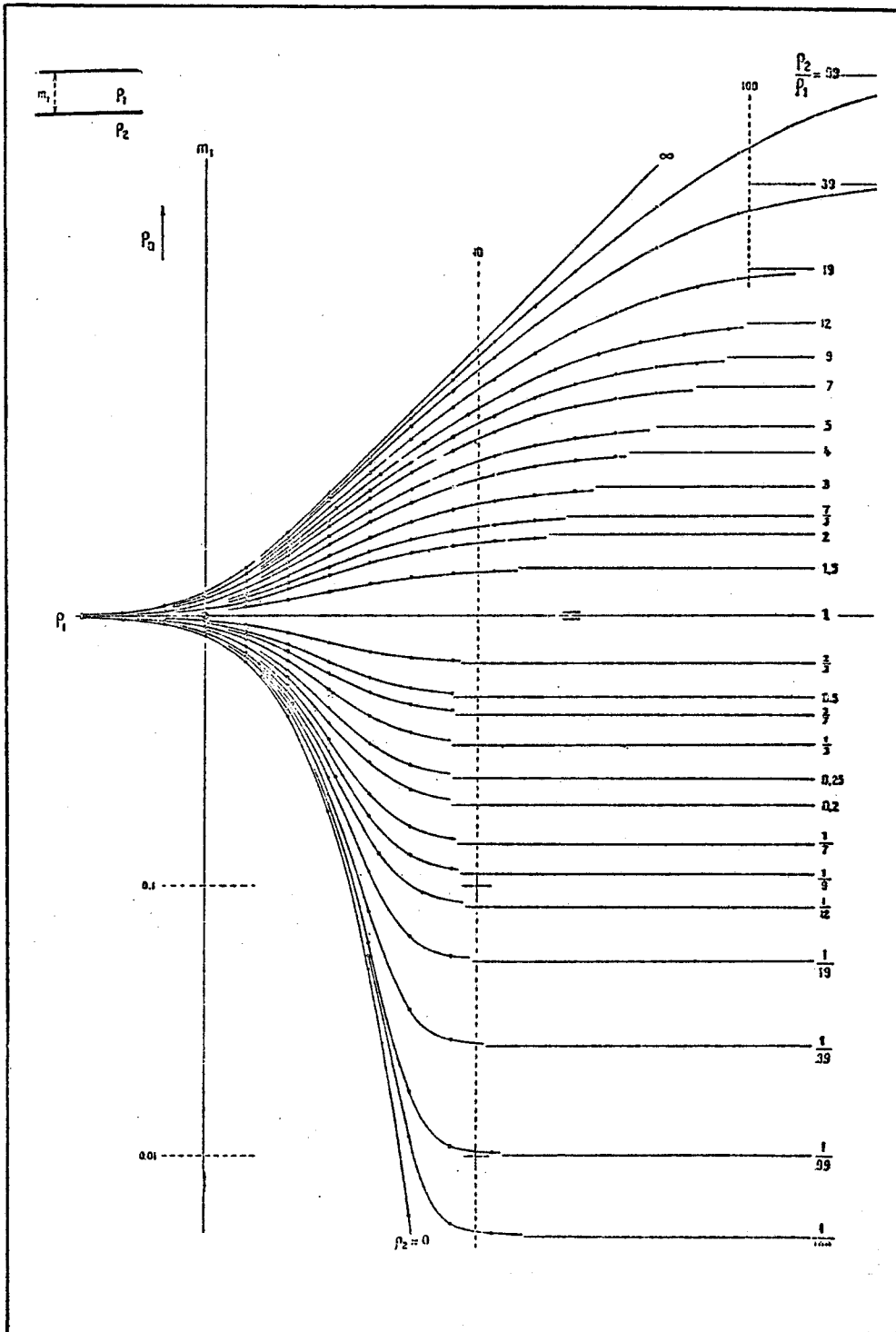
Figure 10. Two-layer master curves for the Schlumberger configuration. (reproduced from Compagnie Generale de Geophysique, 1955).

When there are more than two layers the concept of depth of investigation becomes complex. At this stage it becomes neccessary to invert the field data to theoretical curves and solve for the resistivity and thickness parameters directly.

The maximum array lengths used in the Maui surveys were generally limited to 2,000 meters by terrain, distance to the coast, or small signal. In order to assure reasonable success in obtaining the seawater-saturated rock resistivity, soundings were generally made at elevations not exceeding 250 meters.

VII. RESISTIVITY DEPENDENCE ON POROSITY AND TEMPERATURE

The resistivities of fluid-bearing rocks are mainly controlled by rock porosity, alteration products, fluid temperature, and fluid salinity. The resistivity of fluid-bearing rocks decreases when either the salinity, porosity, or temperature is increased.

A great deal of work has been done correlating resistivity with water content. This work has led to the widespread use of an empirical relation called Archie's law (Keller and Frischknecht, 1966). Archie's law relates the resistivity of a rock to the resistivity of the contained fluid and rock porosity.

$$\rho = \rho_f k \; \phi^{-m} \qquad (36)$$

where:

ρ = bulk resistivity of the rock.

ρ_f = resistivity of the saturating fluid.

ϕ = rock porosity.

k & m = empirically derived constants (dimensionless).

For Hawaiian basalts saturated with freshwater, the fluid resistivity can have a large range of values, yielding a large range of values for the bulk resistivity of freshwater basalt. The fluid resistivity of seawater at room temperature is nearly constant, making the bulk resistivity of seawater-saturated basalt mainly dependant on temperature and porosity. Values of ρ_f, k and m have been estimated for

a large number of seawater-saturated Hawaiian basalts by Rai (1977).
The mean values he found were:

$$\rho_f = 0.21 \text{ ohm-meters}$$
$$k = 5.59 \pm 0.23$$
$$m = 1.42 \pm 0.09$$

substituting these values into Archie's law and solving for porosity
yields:

$$\phi = (.85\rho)^{-.704} \tag{37}$$

Large changes in temperature will produce large changes in the
water-bearing rock resistivities. At moderate temperatures the change
in bulk-rock resistivity is controlled primarily by the change in fluid
resistivity. The fluid resistivity decreases with increasing tempera-
ture because of reduced viscosity of the fluid. Lower fluid viscosity
increases the mobility of ions to flow within the solution, which
increases the fluid conductivity (Keller and Frischknecht, 1966).

A relation for the dependence of resistivity upon temperature for
either a fluid electrolyte or a rock containing a fluid electrolyte
has been developed by Darknov (1962):

$$\rho = \frac{\rho_{20°}}{1 + \beta(t-20°)} \tag{38}$$

where $\rho_{20°}$ is the resistivity of either the fluid or a rock containing the fluid at a reference temperature of 20°. Any reference temperature may be used. The ambient temperature is t and β is the temperature coefficient of resistivity, with a value of about .025 per degree celsius for a NaCl electrolyte.

Substituting Rai's coefficients into Archie's law and substituting the result into Darknov's relation, then solving for temperature yields:

$$t = (\frac{46.956}{\rho})^{-1.42} - 20° \tag{39}$$

where t is the expected temperature for a given porosity (phi), for 20°C seawater saturating basalt of resistivity ρ.

A study on electrical properties of water-saturated Hawaiian basalt from Kilauea Iki on the island of Hawaii by Olhoeft (1977) indicated that relation (39) holds in the temperature range from 0 to 80°C.

VIII. RESULTS

The results of ridge-regression inversion of the Schlumberger sounding data on Maui are presented on the following pages. The presentation consists of the field curve, best-fit theoretical model, model parameters with their standard deviations, and the parameter correlation matrix. Calculated piezometric heads and porosity are given when possible.

The results are given for both coastal corrected and uncorrected models. The modeled apparent resistivity curve (solid line) and correlation matrix are given for the coastal corrected model. The calculated porosity uses the water temperature of the nearest well. The head calculation assumes a 40:1 buoyancy ratio for the freshwater Ghyben-Herzberg lens.

In several cases the correlation coefficients between model parameters is near or equal to unity. In these cases the standard deviations are large (> 100%). When this occurs either one of the parameters is held constant to obtain the standard deviation of the correlated parameter, or the standard deviations are not estimated. In several cases the best-fitting parameters (in the least squares sense) can be calculated but their standard deviations overestimate the actual uncertainty.

1. SOUNDING 1

Sounding 1 (S1) was located 5 kilometers southeast of Lahaina town at 114 meters elevation. The sounding was performed on a sugar cane
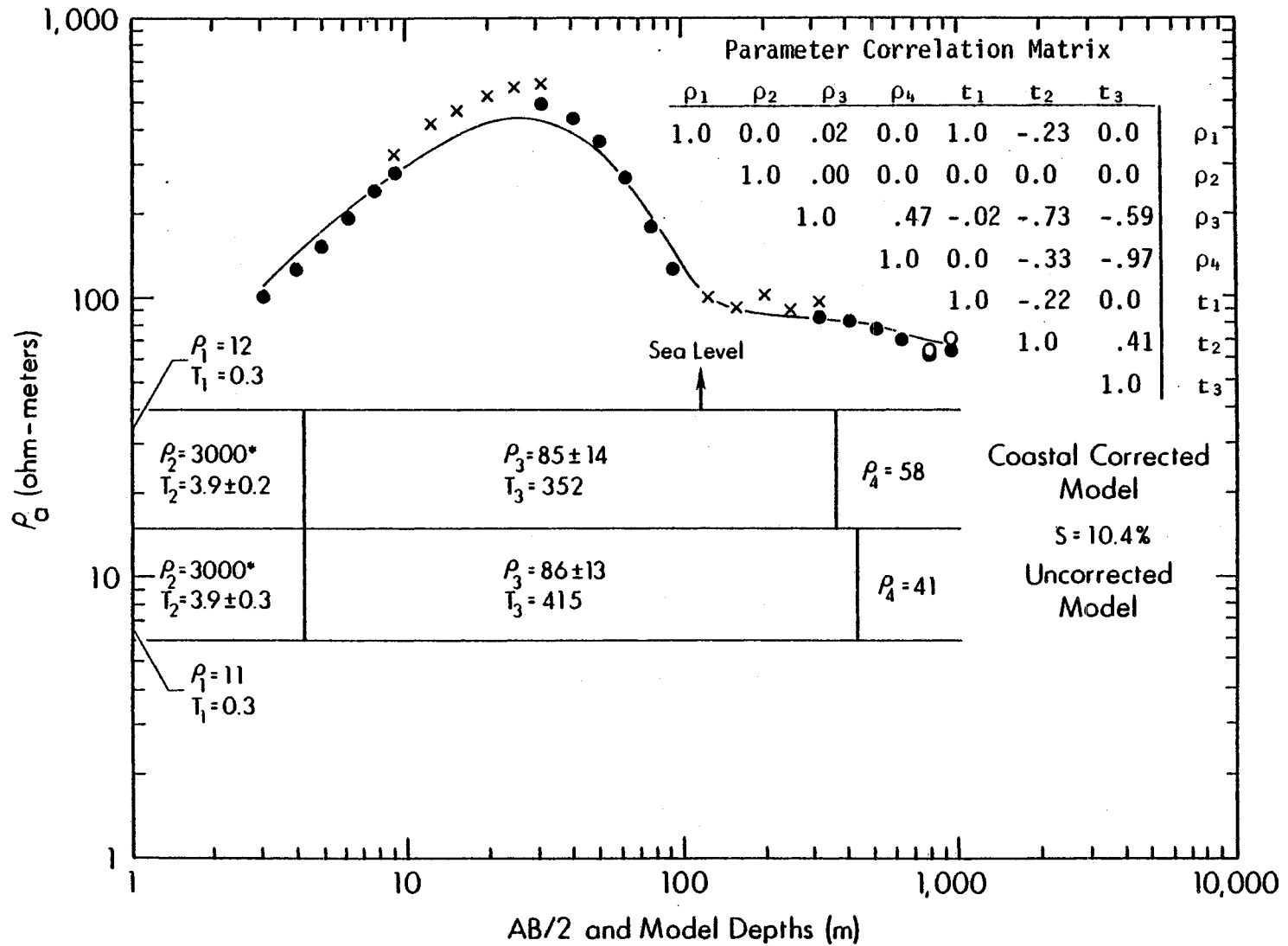
road, oriented perpendicular to the coastline. The Schlumberger spread
ended 244 meters from the coastline, which produces a 10.2% coastal
correction for this point. Two-hundred meters southeast of S1 is an
exposed lava flow of oligoclase andesite (Mugearite) which issued from
Puu Launiopoko (Stearns & Macdonald, 1942).

An offset in the field curve is observed when the MN spacing is
1.2 meters (see Figure 11). The field data were first inverted without
adjusting the offset, but no model could be found which satisfactorily
fit the data. This offset is probably caused by a local heterogeneity
located near one of the potential electrodes. To approximate a one-
dimensional case the offset was shifted down to correspond with the
rest of the field curve.

Four-, five-, and six-layered models were inverted to the adjusted
field data. The five- and six-layered models all diverge by making one
or more of the layer thicknesses equal to 0. The four-layered model can
be made to fit the data by fixing the resistivity of the second layer.
However, regardless of the value used for the resistivity of the second
layer, no theoretical model fits the field curve with a standard
deviation less than 10%. The effect of the offset, which is caused by
some heterogeneity, combined with the relatively large coastal correla-
tion and the scattered values at $AB/2$ = 200 & 300 meters has made the
approximation of a layered earth model questionable.

One piece of useful information which can be gained from S1,
however, is the resistivity of the basement. The depth to the basement
as modeled from the four-layered case is about 356 meters, which is
242 meters below sea level (see Figure 11). The basement resistivities

for the coastal corrected and the uncorrected models is 58 and 41

ohm-meters respectively. The error for the basement resistivity cannot

be accurately estimated due to a high correlation (-.97) with the

thickness of the third layer. Interpreting the basement as basalt

saturated with 20°C seawater and using the porosity relation discussed

in section VI yields a porosity range of 8.2 - 6.4 percent, for the

basalt, from the uncorrected and corrected models respectively.

2. SOUNDING 2

Sounding 2 (S2) was located about 1 kilometer south of Lahaina town.
The sounding was performed on a sugar cane road and was oriented normal
to the coastline at 79 meters elevation. Four-, five-, and six-layered
models were inverted to the field data. The best-fitting model consisted
of five layers. The tie points are all in good agreement. The largest
AB/2 distance came within 91 meters of the coastline, which produces a
20% coastal correction for this point. This large a correction has a
significant effect on the analysis of the bottom two layers.

The resistivity of the first layer was not approached asymptotically
and is highly correlated with its thickness. The inversion tries to fit
a unrealistically thin parameter to the surface layer. The resistivity
of the first layer was therefore held fixed at 27 ohm-m, which was the
asymptotic value obtained from curve matching, and is known to be soil.
The interpretation without the coastal correction gives a half-space
resistivity of 15 ± 6 ohm-meters; with the coastal correction the same
layer is 24 ± 3 ohm-meters. Interpreting the half-space as seawater-
saturated basalt and applying the Ghyben-Herzberg principle yields a
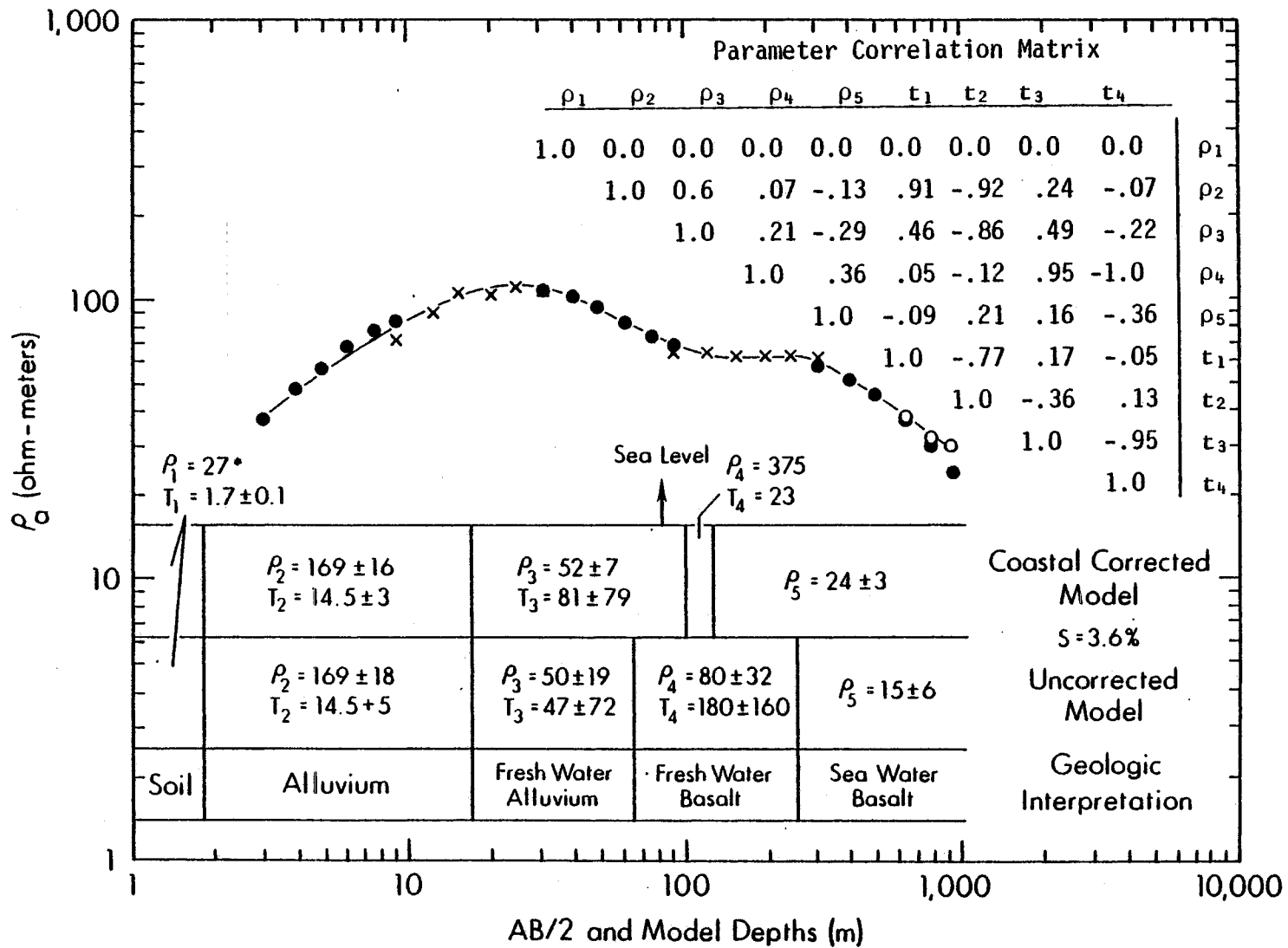
Figure 12. S2 apparent resistivity curve and best fitting models. Note the large parameter changes for layer 4 between the corrected and uncorrected models.

head of 0.9 meters for the corrected model. The geologic interpretation is presented with the geoelectric models in Figure 12. S2 was located on a thick deposit of alluvium which has been mapped by Stearns and Macdonald (1942). The alluvium layer is interpreted as the 2nd and 3rd layers from the Schlumberger sounding, where the 2nd layer is dry and the 3rd layer is wet.

The correlation coefficient between ρ_4 and t_4 for the coastal corrected model is -1.0. Therefore ρ_4 and t_4 are linearly dependent on each other and their standard deviations cannot be independently estimated. The corrected sounding has a 4th layer resistivity of 375 ohm-meters compared to 84 ohm-meters for the uncorrected interpretation. The 4th layer is interpreted as freshwater-saturated basalt. The corrected interpretation is in better agreement with data from well 292, 1 kilometer west of S2. A head between 0.5 and 0.9 meters is reported for well 292, depending on the tide. Archie's law then gives 12% porosity for 20°C seawater-saturated basalt for the basement in the coastal corrected model of S2.

3. SOUNDINGS 3 & 16

Sounding 3 was located 1 kilometer west of Lahaina town at 119 meters elevation. The sounding was performed on a sugar cane road with a 10 inch water pipe running parallel to the road. The effect of the pipe is obvious; the field curve ascends with a slope of 55°, whereas the maximum slope of a Schlumberger curve is 45° for a horizontally layered earth (Kunetz, 1966).
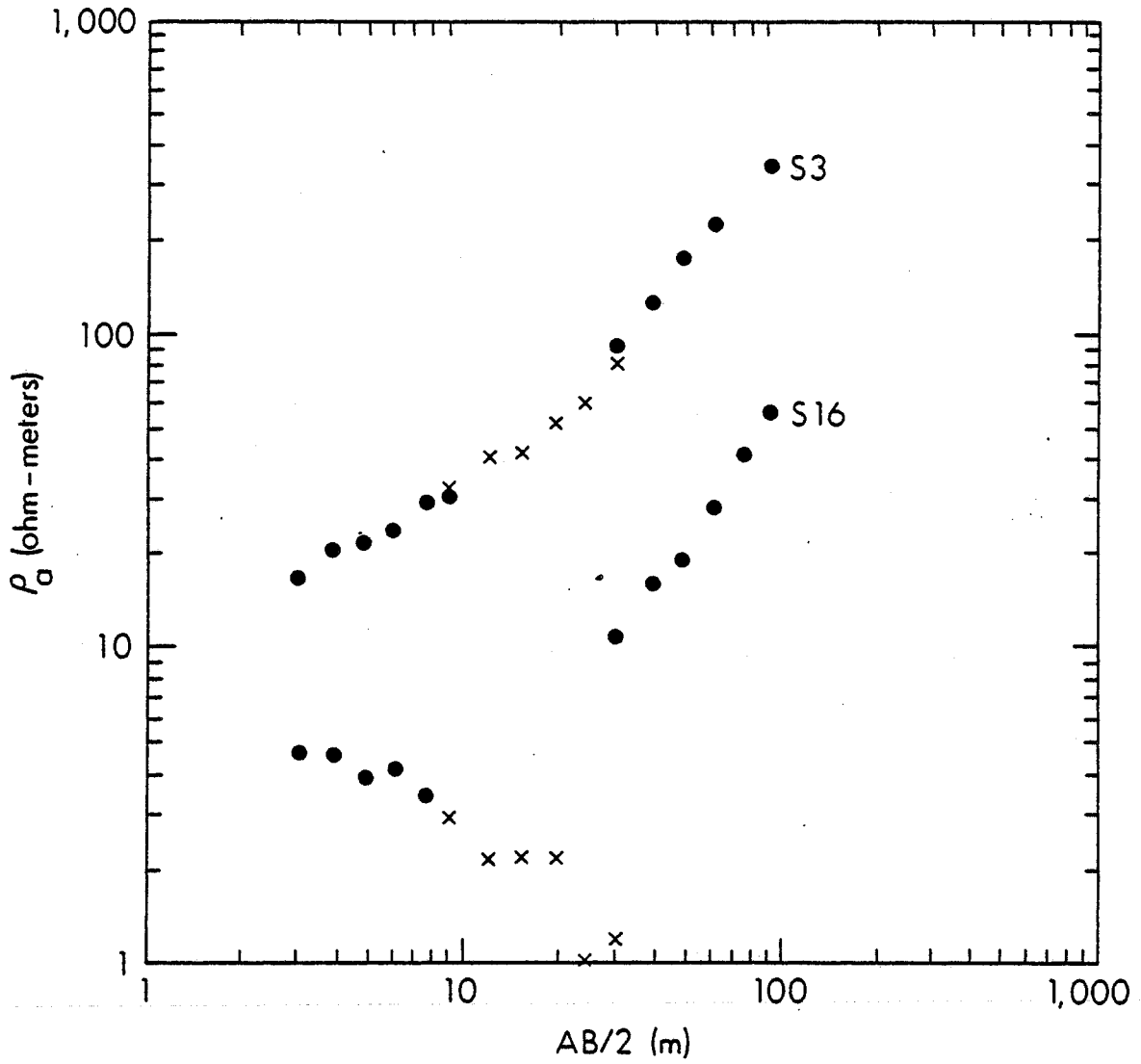
Figure 13. Apparent resistivity curves for S3 and S16. Both curves show the effect of a conductor (water pipe) running parallel to the electrode spread.

Sounding 16 (S16) was located on the Maui isthmus at 152 meters elevation. Although no surface expression of a pipe or railroad track was observed, it is obvious that a buried conductor of some type exists along this road. The field curve ascends with a slope of 60°.

The maximum theoretical slope for a Schlumberger curve, expanded parallel to a highly conductive pipe lying at the surface of a homogeneous half-space is 57° (James Kauahikaua, pers. comm.). Figure 13 shows the field curve for S3 and S16; the erratic points are probably due to intermittent contact with the pipe.

4. SOUNDING 4

Sounding 4 (S4) was located 5 kilometers north of Lahaina town at an elevation of 134 meters. The sounding was expanded normal to the coastline on a sugar cane road. The location was an alternate site for S3 since a pipeline interfered with that sounding. The sounding was 2439 meters from the coast and was not affected by the coastal correction.

The sounding was inverted to 3- and 4-layered models. Eight attemps at fitting a 4-layered model all diverged by one or more parameters approaching 0 or infinity. Three-layered models could be made to fit the data only when one or more of the parameters were fixed. The best fitting three-layered model is obtained when ρ_2 approaches infinity and ρ_3 goes to 0; the error of fit in this case is 7%. Because of the highly resistive second layer, depth of investigation for this sounding is less than 100 meters. Because the depth of investigation is so shallow, no information concerning the hydrology can be inferred at this site.
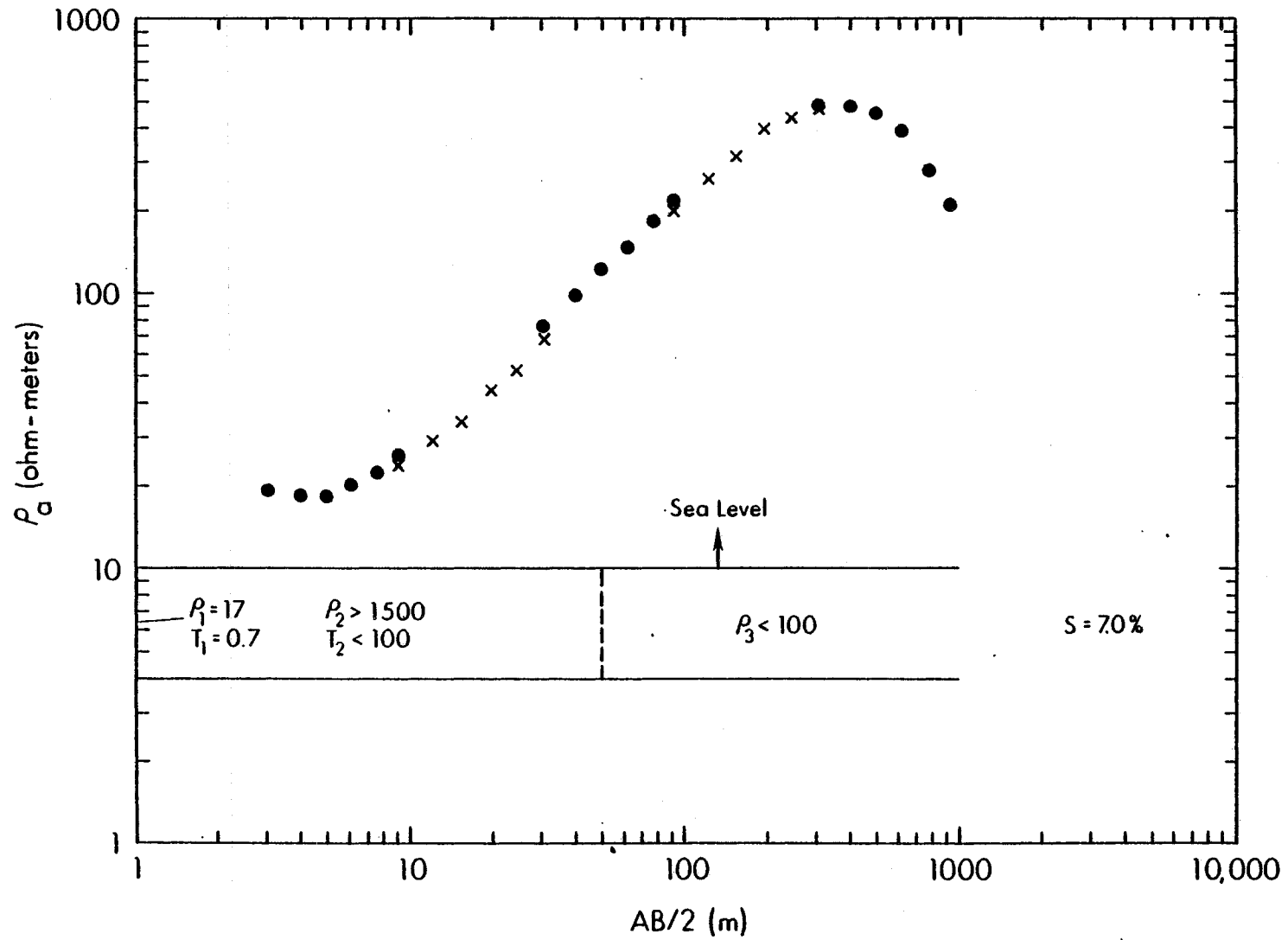
Figure 14. S4 apparent resistivity curve and interpretation.

5. SOUNDING 5

Sounding 5 (S5) was located at the mouth of Olowalu canyon at 61 meters elevation. The sounding was oriented normal to the coastline and the spread ended 137 meters from the coast. Three-, four-, and five-layered models were inverted to the field data. The 4-layered model gives the best fit with a 4.9% error of fit. The coastal corrections at AB/2 values of 762, 610 and 488 meters are 14, 5.4 and 2.6 percent respectively. The coastal correction increased the value of the basement resistivity by 15% and the depth to the basement was decreased by 5% in the 4-layered solution.

Well 10 is located 300 meters west from S5 at an elevation of 50.3 meters. The aquifer for this well is Wailuku basalt. The fresh-water head ranges between 0.9 to 1.3 meters, depending on the tide. The well water temperature is 26°C. The head calculated from S5 is 1.8 meters, which is in good agreement with the well data. The basement resistivity is 7.7 ± 2.7 ohm-meters and is interpreted as seawater-saturated basalt. The calculated porosity is 24% ± 6% for 26°C sea water. The low resistivity basement could also be explained by an elevated temperature.

The third layer is 84 ± 15 meters thick and has a resistivity of 97 ± 53 ohm-meters. This layer penetrates 71.6 meters past sea level and is interpreted as freshwater-bearing basalt. Its value of 97 ohm-meters is low for freshwater basalt and might be explained by high porosity with warm water. The first two layers are soil above alluvium. The geologic interpretation and geoelectric models are presented in Figure 15.

Parameter Correlation Matrix

ρ_1	ρ_2	ρ_3	ρ_4	t_1	t_2	t_3	
1.0	.44	.21	.06	.94	-.27	.11	ρ_1
	1.0	.65	.20	.67	-.79	.21	ρ_2
		1.0	.49	.34	-.97	-.39	ρ_3
			1.0	.10	-.41	-.68	ρ_4
				1.0	-.44	.16	t_1
					1.0	.18	t_2
						1.0	t_3

Sea Level

1,000

100

ρ_a (ohm - meters)

10

1

Soil	Alluvium	Fresh Water Basalt	Sea Water Basalt	
$\rho_1 = 43 \pm 4$ $T_1 = 3 \pm 0.5$	$\rho_2 = 154 \pm 7$ $T_2 = 46 \pm 31$	$\rho_3 = 97 \pm 53$ $T_3 = 84 \pm 15$	$\rho_4 = 7.7 \pm 2.7$	Coastal Corrected Model S = 4.9%
$\rho_1 = 43 \pm 4$ $T_1 = 3 \pm 0.5$	$\rho_2 = 154 \pm 6$ $T_2 = 48 \pm 28$	$\rho_3 = 90 \pm 51$ $T_3 = 88 \pm 19$	$\rho_4 = 6.6 \pm 2.8$	Uncorrected Model

1   10   100   1,000   10,000

AB/2 and Model Depths (m)

Figure 15. S5 apparent resistivity curve, best fit models and geologic interpretation.

6. SOUNDING 6

Sounding 6 (S6) was located 3.7 kilometers from the coast at 427 meters elevation. The sounding was performed in the foothills behind Lahaina town. No coastal correction was needed for this sounding. Three- and four-layered models were inverted to the field data with four-layered models giving a significantly better fit. Three important phenomena are exemplified by this sounding.

1. The principle of suppression: the second layer (338 ohm-m) has a resistivity intermediate between the layer above and the layer below it, which gives the field curve the shape of a continually ascending branch (see Figure 16). Had the second layer (25 meters thick) been deeper (> 75 meters) its effect on the field curve would be practically indistinguishable from that of a three-layered curve.

2. The depth of resolution: the resistivity of layer four encountered at 269 meters depth cannot be resolved, even though the Schlumberger array was expanded to AB = 1829 meters. The only thing which can be said about the resistivity of ρ_4 is that it is less than 600 ohm-meters. Layer four is interpreted to be freshwater basalt which implies that a lower resistivity layer should underly it. It is possible that the effect of a conductive half-space is present to some degree in the data, but it is not possible to evaluate what that effect is without additional data.
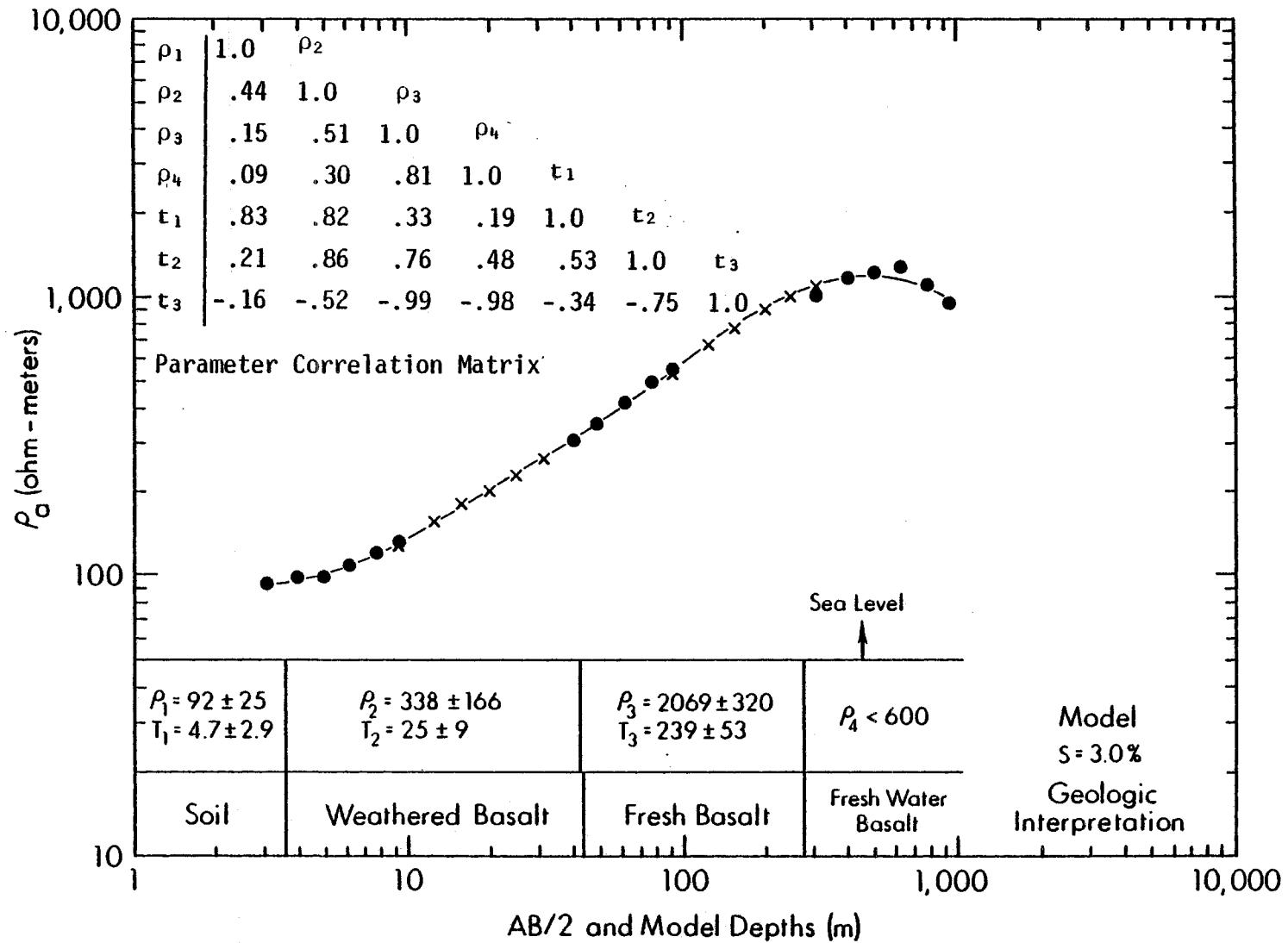
Figure 16.   S6 apparent resistivity curve, best fit model and geologic interpretation.

3. The third phenomenon is partial saturation. If the bottom

   layer is interpreted correctly as freshwater basalt and it

   is assumed that the pore space is 100% filled with water,

   then the freshwater head observed at this location would

   be an unlikely 158 meters above sea level. The more

   reasonable interpretation is that at a depth of 269 meters

   the critical saturation of basalt has been encountered.

   As discussed in section I, increasing the amount of fluid

   in the pore space after the critical saturation has been

   reached only slightly decreases the bulk resistivity.

Figure 16 shows the field curve, best-fit model with standard deviations

and the most reasonable geologic interpretation.

7. SOUNDING 7

Sounding 7 (S7) was located about 1.5 kilometers from Puu Kilea

near Lahaina. Puu Kilea is a post-erosional cone of geothermal interest.

The sounding was oriented parallel to the coast at 114 meters elevation.

The sounding was located 701 meters from the coast. The basement

resistivity was increased by 13% after application of the coastal

correction. The field data for S7 is scattered and there are significant

differences at the tie points. The best fitting theoretical curve has

a RMS error (s) of 11.6%. This implies that the earth is not homogeneous

and/or the assumption of horizontal layering has been violated. The

field curve was nonetheless inverted to 3- and 4-layered models. Five

different 4-layered models were inverted by holding one or more of the

parameters fixed. Results showed that the third layer was being fit to
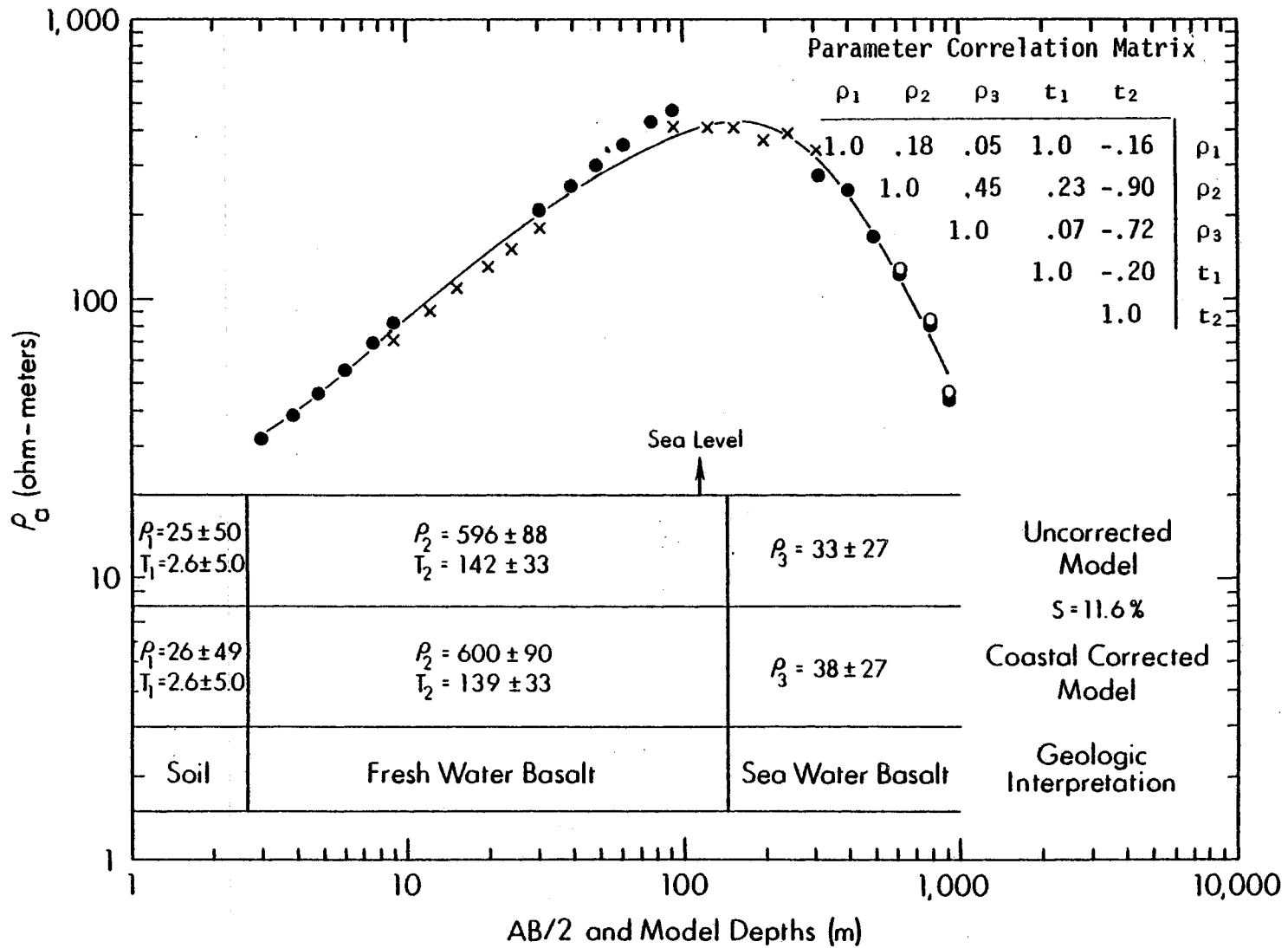
Figure 17. S7 apparent resistivity curve, best fit models and geologic interpretation.

the noisiest portion of the curve, between $AB/2$ = 91.4 to 304.8 meters. When a 3-layered model was inverted to the data, the goodness of fit was approximately the same and the model was not being forced to fit the noisy part of the curve. The 3-layered model also provides a more geologically reasonable solution.

The coastal corrected solution yields a basement resistivity of 38 ± 27 ohm-m and is interpreted to be seawater-saturated basalt with 10% porosity. The depth to this basement is 142 meters which would yield a head of 0.7 meters. The first and second layers are interpreted as alluvium and freshwater basalt respectively. Well 292 at 134.7 meters elevation is located 2.6 kilometers east of S7. The measured head of well 292 is 0.46 to 0.88 meters in Wailuku basalt, which is in good agreement with the 3-layered solution.

8. SOUNDING 8

Sounding 8 (S8) was located near the mouth of Ukumehame canyon at 23 meters elevation. The sounding was expanded on sugar cane road oriented parallel to, and 430 meters from the coast. Four- and five-layered models were inverted to the field curve. The 4-layered model gives the best fit. The 5-layered model did not converge. The coastal correction increases the basement resistivity by 11% from 3.5 to 3.9 ohm-meters, and decreases the depth to the basement by 1.0%.

The basement resistivity for S8 is the most conductive layer measured on Maui. Well 12 located 1.6 kilometers west of S8 reports a head of 1.0 to 2.0 meters with a water temperature of 33°C. The aquifer is thin-bedded Wailuku basalt lava flows. The calculated head for S8 is
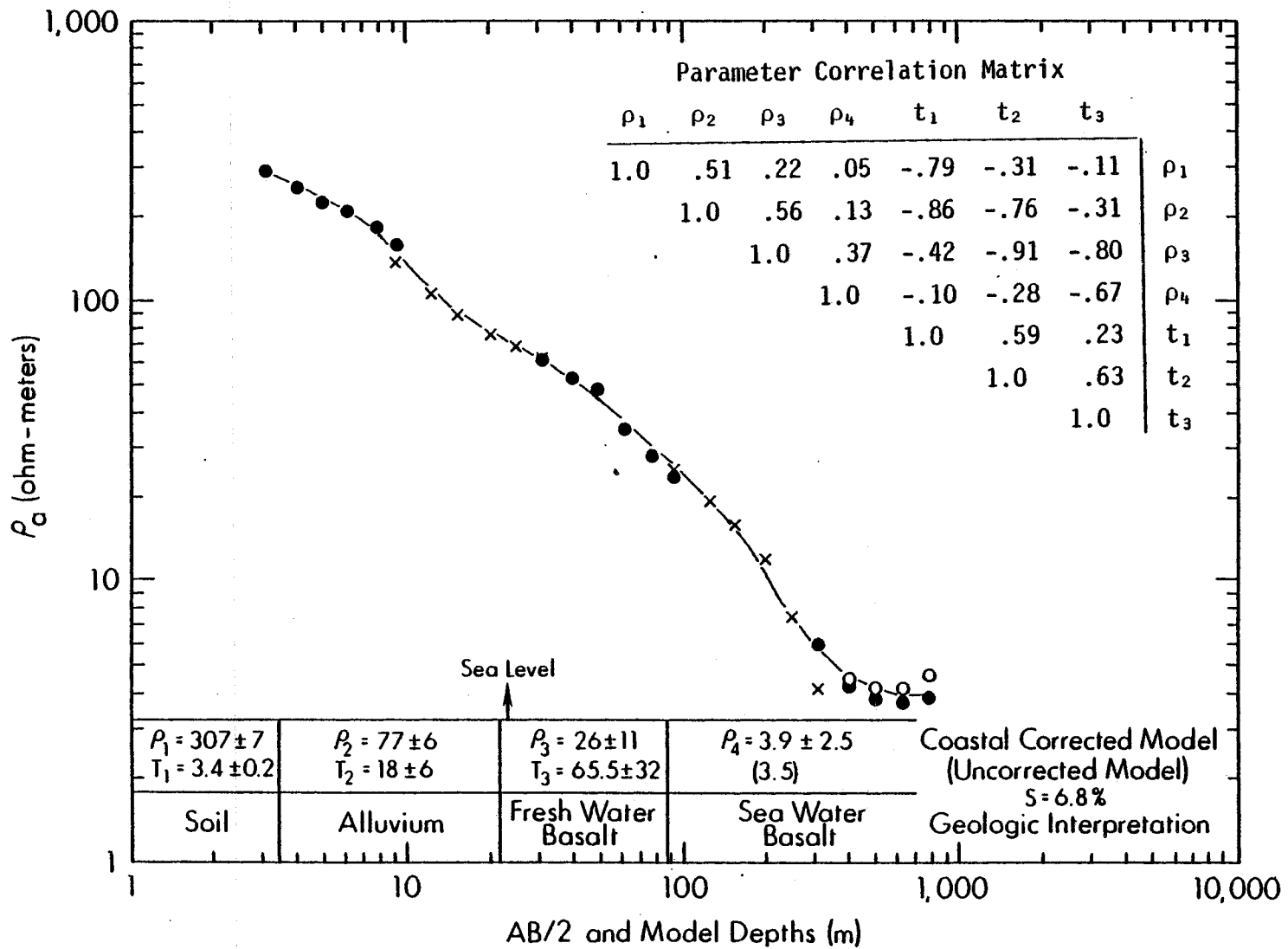
Figure 18. S8 apparent resistivity curve, best fit models and geologic interpretation. The basement resistivity is the lowest measured on Maui.

1.6 meters, in excellent agreement with the well data. The third layer of S8 is 26 ± 11 ohm-m and is 65.5 meters thick. This layer is too thick to be weathered basalt or a buried soil layer, yet the resistivity is very low for cold, freshwater basalt. The first two layers are interpreted as soil over alluvium.

The upper surface of the third layer (26 ohm-m) corresponds in depth to the surface of the calculated water table. This is the only sounding with this correspondence. The temptation is to interpret the interface between the 2nd and 3rd layer as a boundary between cold and warm freshwater basalt. It is more likely, however, that the bottom of the alluvium layer coincides with the top of the freshwater lens at this site. This interpretation is supported by the results of S12 and S21 which are also located near Ukumehame canyon.

A bulk porosity of 45% for 20° seawater-saturated basalt, or 35% porosity for 33° seawater-saturated basalt could explain the conductive basement measured at Ukumehame. Using the average bulk porosity range of 15% to 25% (Peterson and Segal, 1974) for Hawaiian basalt, the temperature calculation is 62 to 153°C for the coastal corrected model and 71 to 171°C for the uncorrected model.

9. SOUNDING 9

Sounding 9 (S9) was located 1.8 kilometers northeast of Maalaea town at 20 meters elevation. The sounding was oriented normal to the coastline and approached a post-erosional cone (Puu Hele) to the north. The Schlumberger spread ended 244 meters from the coast. A large offset in the field curve occurs at AB/2 = 10 to 30 meters and when MN = 1.2

meters. This is probably due to a heterogeneity near one of the potential electrodes. The data for MN = 1.2 meters was not used in the inversion.

Four-, five-, and six-layered models were inverted to the field data with the 4-layered models giving the best fit. A severe problem of equivalence existed for all the parameters except the basement resistivity. This problem is reflected in the correlation coefficient matrix presented in Figure 19. Except for the basement resistivity every parameter is highly correlated (> .90) with one or more of the other parameters. The parameters with large correlation coefficients are linearly dependent upon each other. The field curve asymptotically approaches the resistivity of the basement, which allows the resistivity of this layer to be determined uniquely. This is also reflected in the correlation matrix, where the highest correlation coefficient for the basement resistivity parameter is -.30. This parameter is therefore nearly linearly independent of all the other parameters.

Since most of the parameters are correlated it is difficult to approximate their errors. By fixing one of the parameters it is possible to estimate what the errors of the other parameters are, with respect to the fixed parameter. Figure 19 shows the 4-layered solution with the second resistivity fixed at 11 ohm-m. The shallow second layer is probably sediment and is of no interest hydrologically or geothermally. By fixing this layer, information can be gained about the deeper layers.

The third layer resistivity and thickness are perfectly correlated (cc = -1.0). Using the principle of equivalence (Keller & Frischnecht, 1966) the range of resistivities for the 3rd layer is 300 to 750 ohm-m.
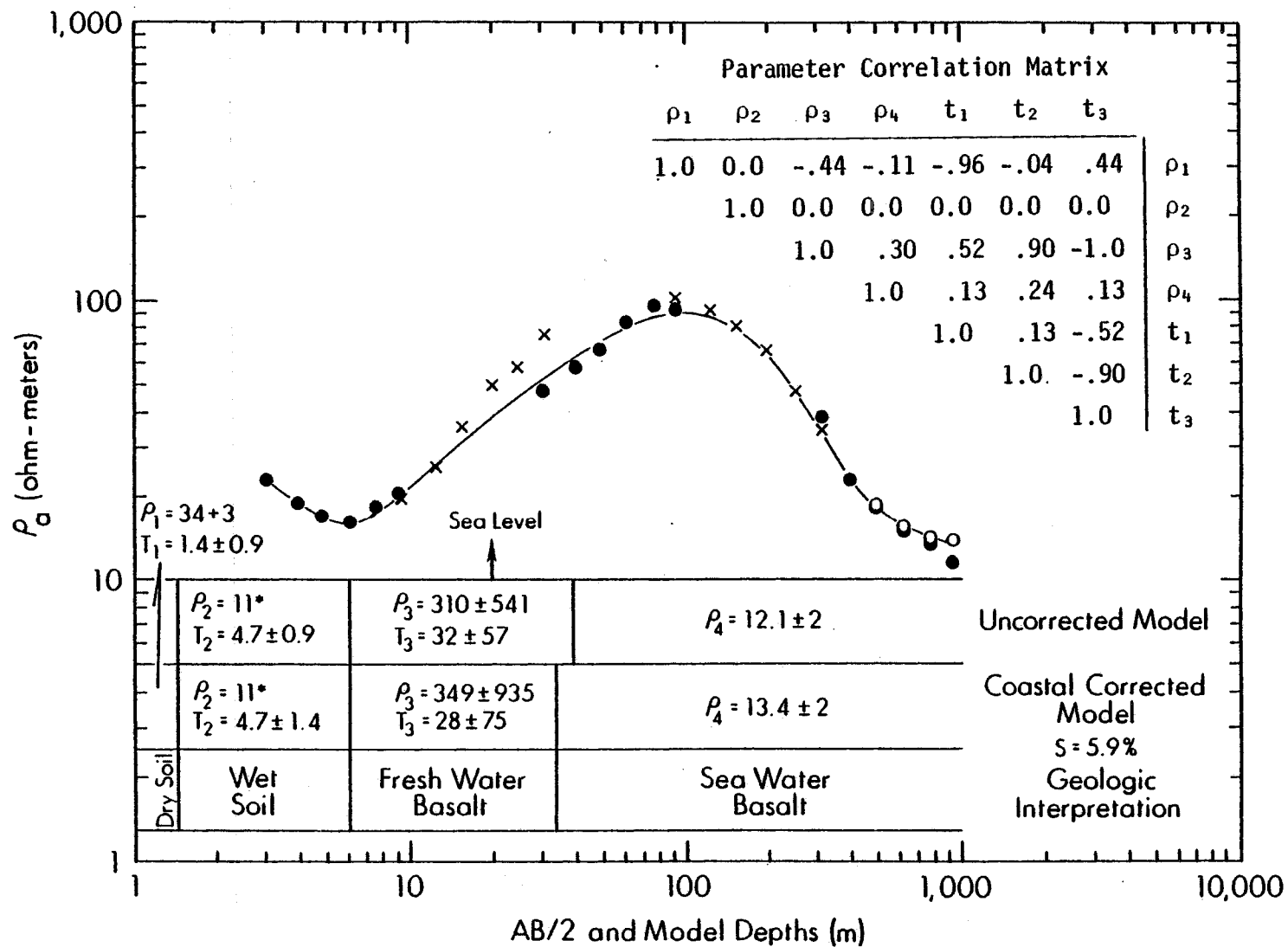
Figure 19. S9 apparent resistivity curve and geologic interpretation. The data from 10 to 30 m AB/2 (x's) were not used during the inversion, see text.

The range of thickness is 13 to 50 meters. These resistivity values
are typical for freshwater-bearing basalt (Zohdy and Jackson, 1969) and
the thicknesses yield a range of heads of .03 to 0.9 meters.

Well 110 is located 182 meters west of S9 at 101 meters elevation
and penetrates Wailuku basalt at 14.9 meters depth. A freshwater head
of 2.0 meters is observed in this well. Since S9 is only at 20 meters
elevation it is not unreasonable that the freshwater head is less than
0.9 meters. Interpreting the basement in S9 as 20°C, seawater-saturated
basalt, its resistivity of 13.3 ohm-m yields a porosity of 18%.

10. SOUNDINGS 10 AND 11

Soundings 10 and 11 (S10 & S11) were located at the northern end
of West Maui. S10 was at 171 meters elevation; S11 was at 229 meters
elevation. The coast had a negligible effect on both soundings. Both
curves have similar shape, and were interpreted using 5-layered models.
Except for the third layer in S10 no layer asymptotically approaches its
resistivity. Both curves are plagued with equivalence problems. S11
exhibits a 92 ohm-m jump in apparent resistivity at the 30.5 m $AB/2$
spacing and a 25 ohm-m jump at the 91.4 m $AB/2$ spacing. These jumps are
substantial, meaning the assumption of horizontal layering has been
violated. Even when the points are shifted to approximate one dimension-
ality the high correlation between parameters makes it impossible to
estimate independent standard deviations. The only information which can
be gained from S11 are the parameters of the surface layer (160 ohm-m
and 6.1 m thick) and that the resistivity of the basement is less than
60 ohm-m.
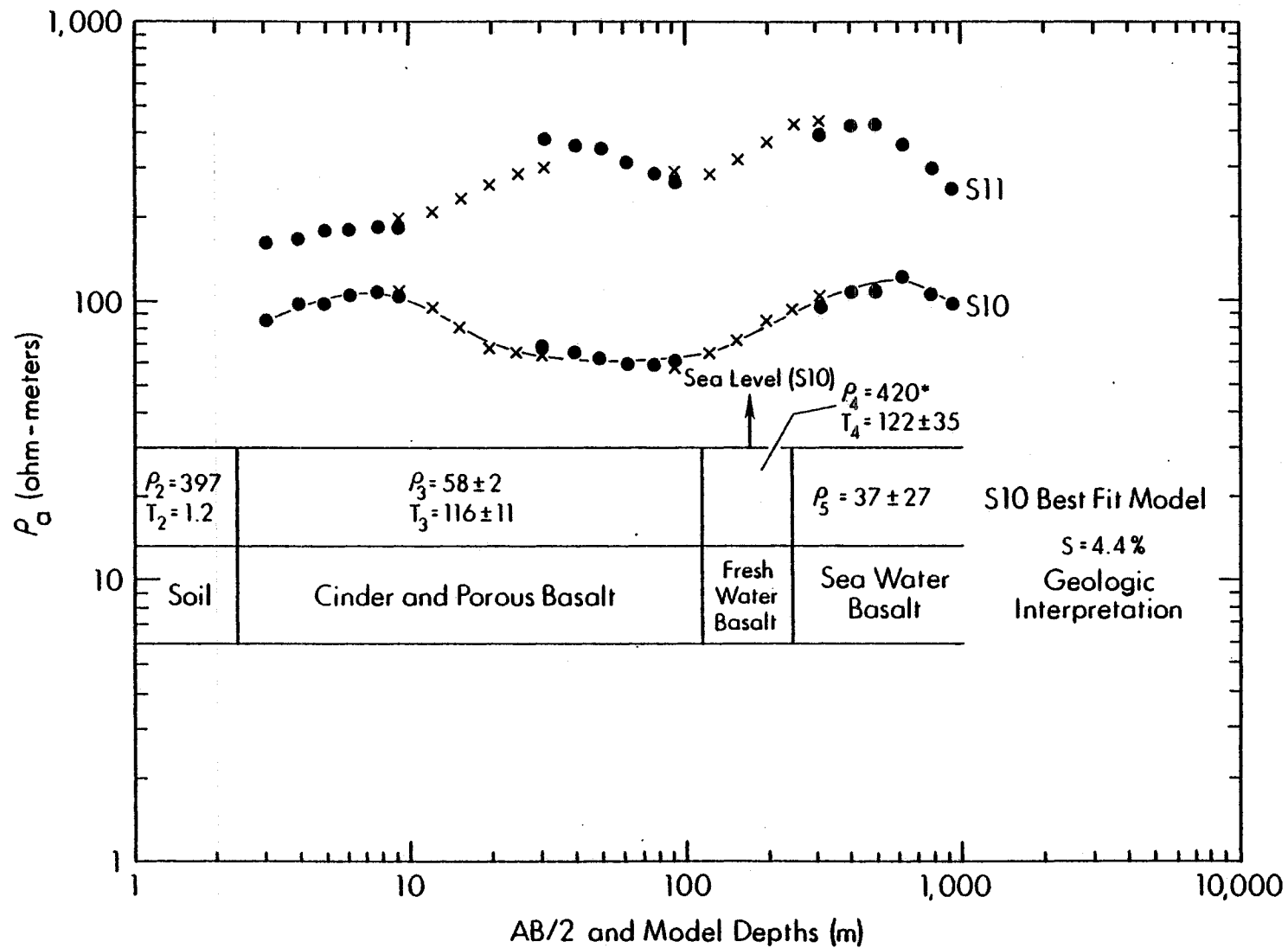
Figure 20. Apparent resistivity curves for S10 and S11. The best fit model and geologic interpretation is given for S10 only, for explanation see text.

More information is gained from S10 by comparing well data. Two wells are located 5.6 and 7.2 kilometers east of S10. Well 1 and 318 are at 78.3 and 273 meters elevation respectively (see Figure 1). Well 1 penetrates Wailuku basalt at 26.5 meters depth and yields a static head of 0.8 meters. Well 318 yields a static head of 1.8 to 2.1 meters, also in Wailuku basalt. Water temperature in both wells is 21°C.

The correlation coefficient between ρ_4 and t_4 is -1.0. Only the ratio ρ_4/t_4 can be determined. Resistivities ranging between 200 and 600 ohm-m can be assigned to ρ_4 without altering the fit of the curve as long as the ratio ρ_4/t_4 remains nearly the same. By fixing ρ_4 to 420 ohm-m this sounding yields a calculated head of 1.7 meters, and a basement resistivity of 37 ± 27 ohm-m. Interpreting the basement as seawater-saturated basalt yields a porosity range of 6 to 20% for 20°C water temperature.

A thick conductive third layer is present in both soundings. A comparison of well logs suggest that this layer is a thick sequence of alternating cinder and basalt layers of high porosity. Although the well logs do not indicate whether this unit carries water or not, the inversion results imply that the level of critical saturation is achieved.

11. SOUNDING 12

Sounding 12 (S12) was located at the mouth of Ukumehame canyon at 44 meters elevation, near Ukumehame stream. The sounding was oriented normal to, and 945 meters from the coastline. The surface layer at this site is consolidated alluvium and is observed to be at least 8 meters

thick in a nearby stream cut. The field curve is generally smooth except at 3 points, AB/2 = 152.4, 234.8 and 487.7 meters. Two freshwater reservoirs were located 300 meters north of S12 and the array was expanded along the service road to these reservoirs. All the piping associated with the reservoirs is made of p.v.c. plastic, and the flood gates are made of iron. Whether the noisy points are due to the reservoir structure or to other heterogeneities has not been determined. The only effect of these points on the data inversion was to slightly increase the root-mean-square-error (S).

Three- and four-layered models were inverted to the field data. The 4-layered inversion reduces the third layer thickness to 0 m, resulting in a 3-layered model. The coastal effect increases the base- ment resistivity from 3.7 to 4.3 ohm-m and decreases the depth to the basement by 2%. The best-fit models with geologic interpretations are presented in Figure 20. The second layer is interpreted as freshwater- bearing basalt and the basement is interpreted as seawater-saturated basalt. This model is virtually identical to S8 located 748 meters to the east. The low resistivities for the basalt layers are probably due to elevated temperatures as explained for S8. The calcualted head for S12 is 3.6 meters and is probably high in this area due to the close proximity of Ukumehame stream. S12 was expanded along the Ukumehame stream bank. Additional evidence for elevated temperatures in this area was obtained from S21 which is located near the warm-water well (W12).
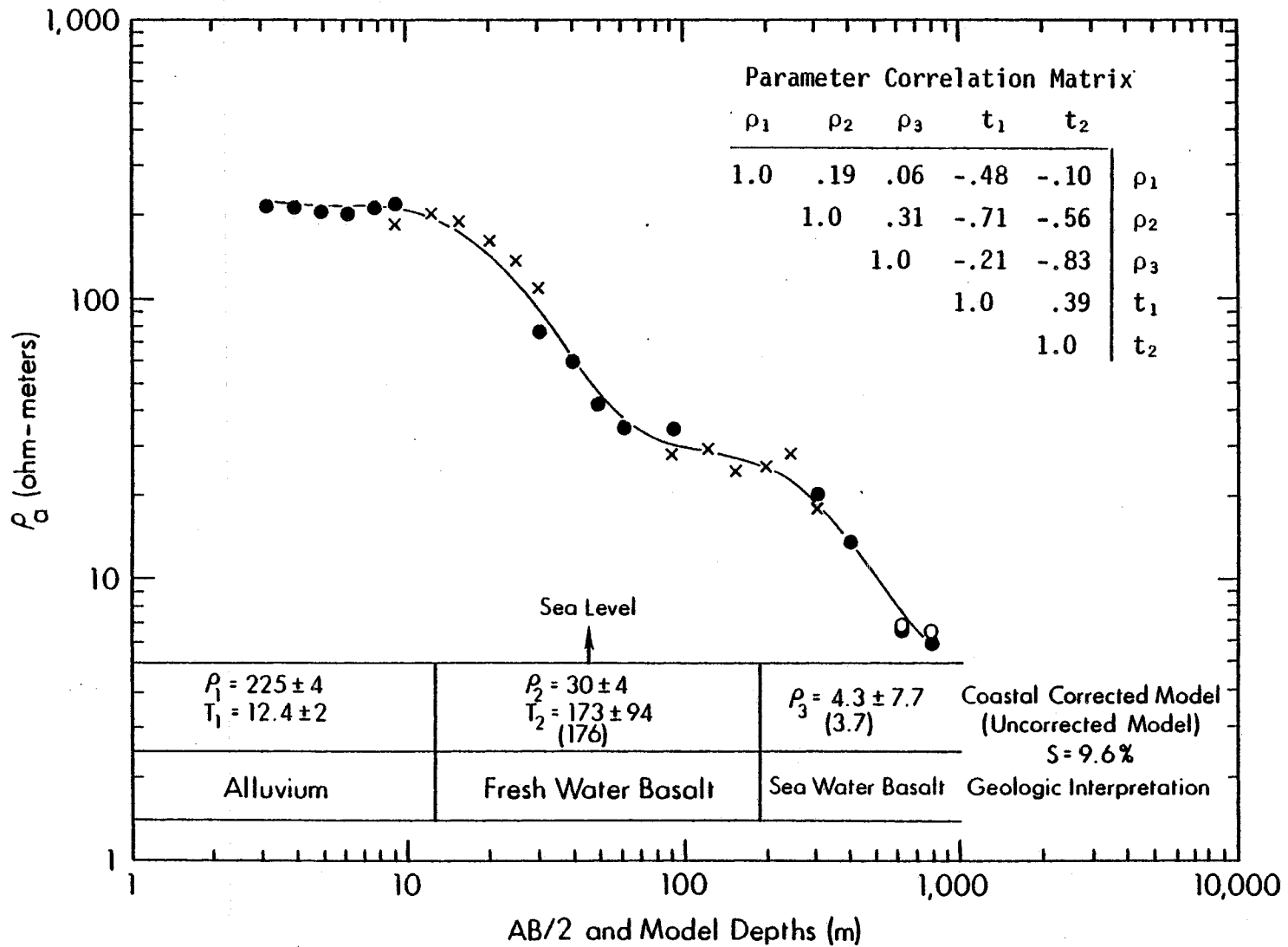
Figure 21. S12 apparent resistivity curve, best fit models and geologic interpretation, note the conductive basement.

12. SOUNDING 13

Sounding 13 (S13) was located near the southwest rift zone of Haleakala at 546 meters elevation. The sounding was located 5.3 kilometers from the coastline. The coastal correction has no effect on this sounding. This area is close to the site of the most recent eruption on Maui (1790). The eruption issued from two vents, the closest being 1.5 km west of S13.

The measured apparent resistivities are very high, ranging between 1,300 and 12,000 ohm-m. The seawater-saturated basalt layer was not encountered with this sounding, due to insufficient depth of penetration. Without information on the seawater-saturated basalt layer, hydrological and geothermal conclusions are more speculative.

Standard deviations are estimated for only three parameters because all other parameters are highly correlated (cc > .90). Since the depth to the seawater interface cannot be determined, it is not possible to calculate the freshwater head at this location. The deepest layer is interpreted to be freshwater-bearing basalt; its resistivity is 865 ohm-meters, which is high for basalt containing freshwater. This high resistivity implies that the water is cold and contains few dissolved solids. The water is possibly of high quality in this area but additional work is required to assess the volume of freshwater present.

Assuming a seawater basement exists at depth for this site, then to uniquely resolve its resistivity a minimum AB separation equal to eight times the elevation, or 4,368 meters would be required. Since the resistivity contrast is so large (about 1000) a AB = 10,000 meters is more likely in order to resolve the seawater-saturated basement resistivity.
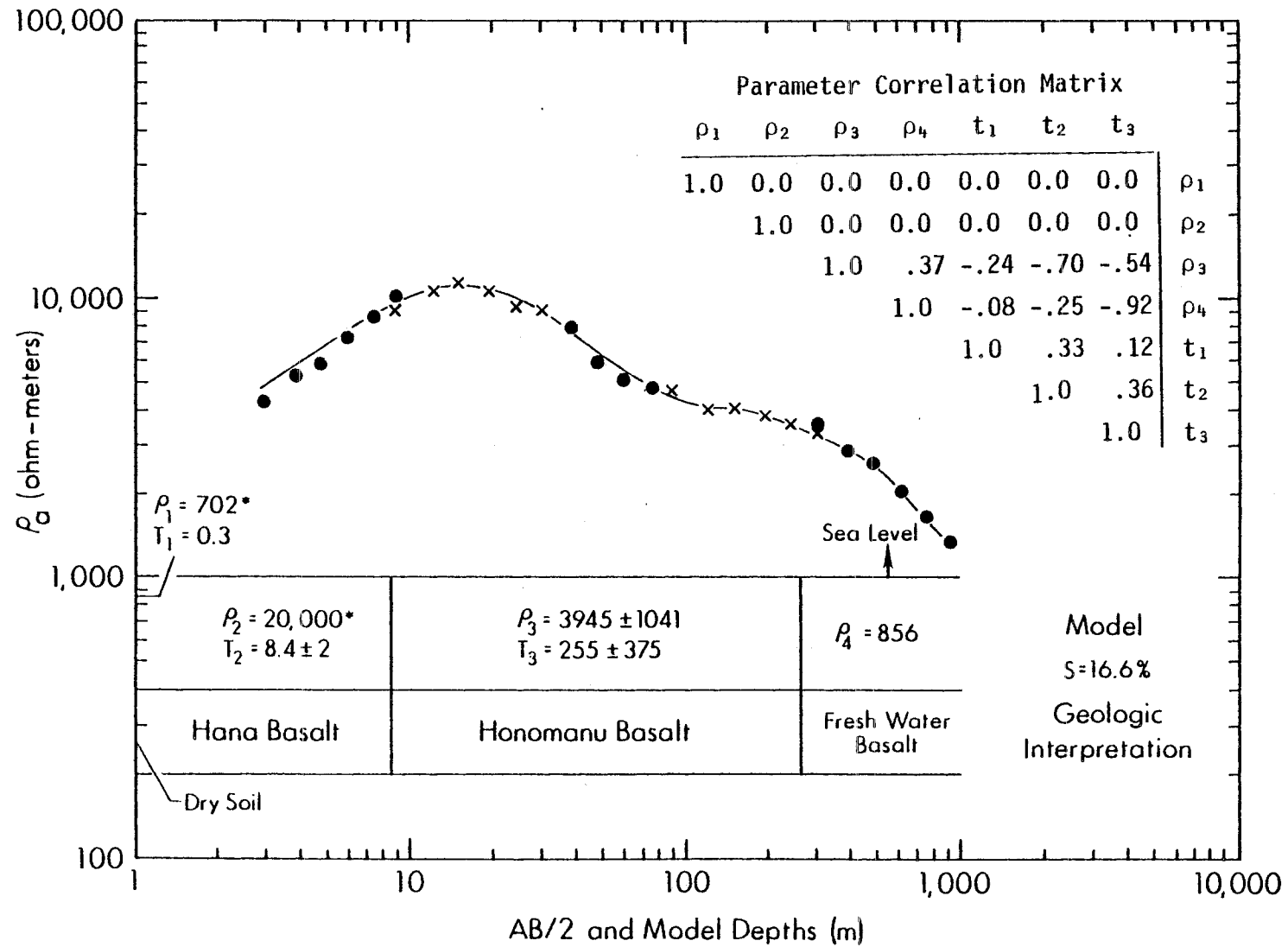
Figure 22. S13 apparent resistivity curve , best fit model and geologic interpretation, note high RMS error (S).

13. SOUNDING 14

Sounding 14 (S14) was located on the east rift zone of Haleakala
on the Hana ranch. Work was performed in a cow pasture with dozens of
grazing cattle. At the 487.7 meters AB/2 spacing a bull got tangled in
the wire. This spooked the bull and he took off running with the wire
tangled around his legs. The bull pulled the reel of wire out of my
hands and I watched the reel of wire bounce down the pasture. After the
wire was retrieved we relocated the center point up slope to acquire
deeper information. The apparent resistivity values at 610 and 762
meters AB/2 correspond to the new center point.

Four-, five-, and six-layered models were inverted to the field
data. Five-layered models provide the best fit. A large jump at the
AB/2 = 304.8 meters was adjusted with an upward shift. The inversion
does not accept this shift very well, as the resulting 'bump' in the
field curve poorly fits the 5-layered model. The inversion attempts
to put a conductor-resistor sequence in the data to fit the bump (see
Figure 22). When a 6-layered model is inverted to the data, however,
all thickness parameters are forced to be very thin in an alternating
conductor-resistor sequence.

The following table shows the effect of fixing the basement
resistivity for a 5-layered model. This is the type of model which best
fits the data, with small variations in the goodness-of-fit due to
variations in the basement resistivity.

The basement resistivity is less than or equal to 150 ohm-m. By
fixing the basement resistivity it is not possible to calculate the
correlation coefficient for this parameter. By inspection of Table 1
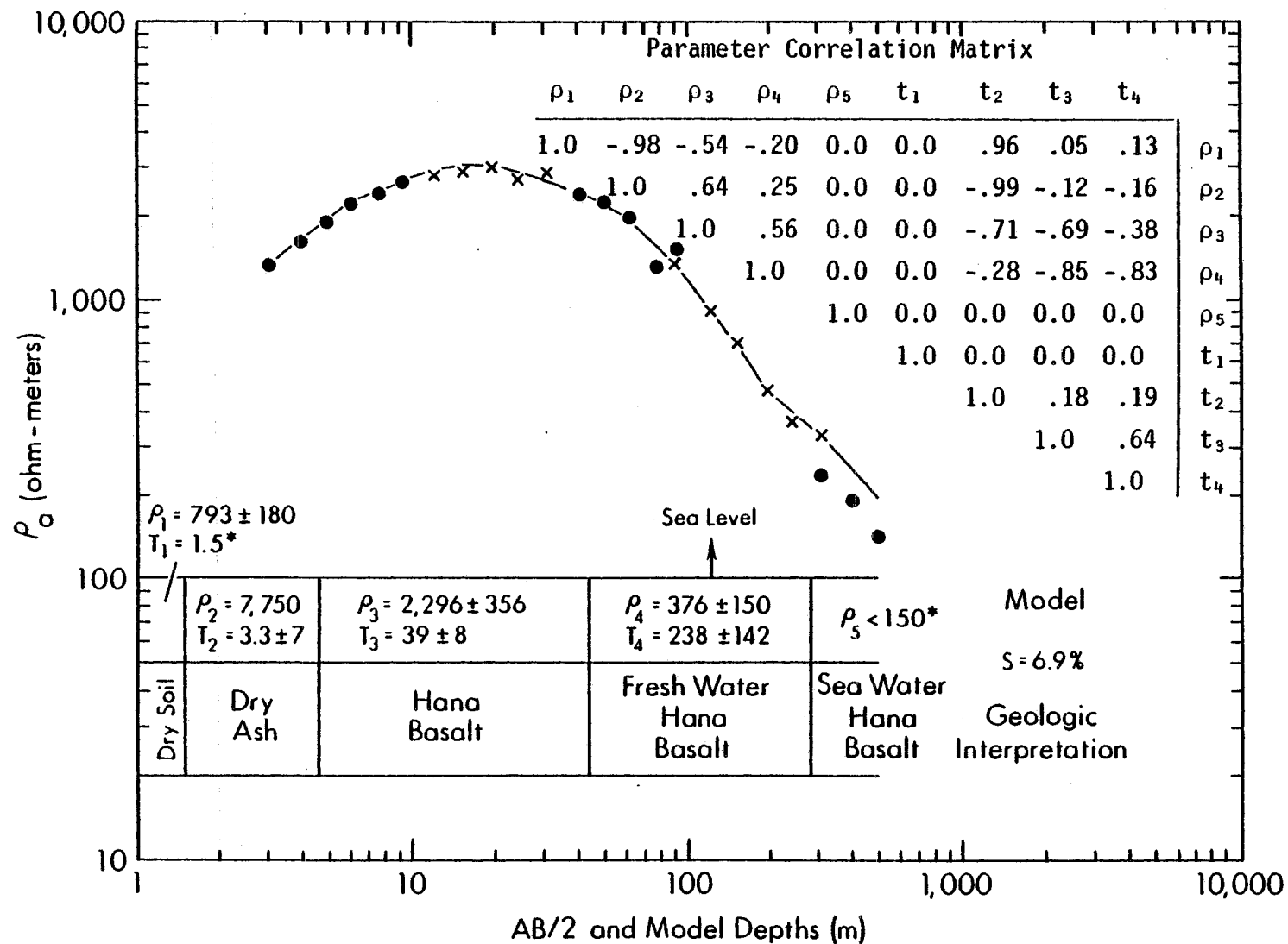
Figure 23. S14 apparent resistivity curve and geologic interpretation. The last 3 data points were shifted upward during the inversion.

Table 1

Basement ρ	S	F.W. Basalt (ohm-m)	Head (m)
150	9.1%	460	1.0
100	9.2%	405	2.4
30	9.3%	375	4.0
1	9.3%	369	4.7

it is obvious, however, that this parameter is correlated with the resistivity of the layer above it. Table 1 shows that the resistivity of the fourth layer is 369 to 460 ohm-m, with the higher values corresponding with the higher values of the basement resistivity. The significance of this is that the resistivity of the fourth layer is in the range of expected values for cold, freshwater-bearing basalt (see Summary). The thickness of the fourth layer is also dependent on the basement resistivity. Assuming that the basement is cold, seawater-saturated basalt, the expected value of the basement is about 30 ohm-m. Using this value a speculative estimate of 4 meters can be calculated for the freshwater head at this location.

14. SOUNDING 15

Sounding 15 (S15) was located at the end of Haleakala's north rift zone, along Manawaiiao stream, at 99 meters elevation. The field data were inverted to 3- and 4-layered models, with the 4-layered model providing the best fit. The sounding was performed on a pineapple field

Parameter Correlation Matrix

	ρ_1	ρ_2	ρ_3	ρ_4	t_1	t_2	t_3	
	1.0	−.76	−.21	−.06	0.0	.56	.11	ρ_1
		1.0	.30	.09	0.0	−.72	−.16	ρ_2
			1.0	.35	0.0	−.70	−.59	ρ_3
				1.0	0.0	−.23	−.85	ρ_4
					1.0	0.0	0.0	t_1
						1.0	.39	t_2
							1.0	t_3

$\rho_1 = 170 \pm 17$
$T_1 = 0.6*$

Sea Level

100 — ρ_a (ohm-meters)

$\rho_2 = 302 \pm 4$
$T_2 = 18.4 \pm 1$

$\rho_3 = 65 \pm 5$
$T_3 = 194 \pm 55$

$\rho_4 = 10.5 \pm 8$
(9.2 ± 6)

Coastal Corrected Model
(Uncorrected Model)

S = 4.4 %

Fresh Water
Kula Basalt

Fresh Water
Honomanu Basalt

Sea Water
Honomanu
Basalt

Geologic Interpretation

Soil

AB/2 and Model Depths (m)

Figure 24. S15 apparent resistivity curve, best fit models and geologic interpretation.

road. The surface layer is a thin soil layer, 0.6 to 3.0 meters thick, but no measurements were taken for AB/2 less than 3 meters, making the resistivity and thickness of the surface layer difficult to resolve. The next 3 layers are well resolved and are the layers of geothermal and hydrological interest.

The coastal correction increases the resistivity of the basement from 9.2 to 10.5 ohm-meters, but all other parameters are unaffected. Using nearby well-log data (W31), the following geologic interpretation has been made: soil, freshwater-bearing Kula basalt, freshwater-bearing Honomanu basalt, and seawater-saturated Honomanu basalt. This interpretation is shown in Figure 24.

The calculated freshwater head is 2.7 meters. Wells in the area average about 1.5 meters of head. A local high head is probably due to the close proximity of Manawaiiao stream. The calculated porosity is 21% for this sounding. This high proosity is reasonable for Honomanu basalt. Stearns and Macdonald (1942, p. 67) report that Honomanu basalt is "...highly permeable and freely yields basal water to wells." All layers contain moisture from pineapple irrigation and high rainfall. The value 65 ± 5 ohm-m for Honomanu basalt is quite low. This result is difficult to explain. The layer is too thick (195 m) to be a buried ash or sedimentary layer. The freshwater-bearing Kula basalt and the seawater-saturated Honomanu basalt both suggest about 20% porosity for 20°C water. A sandwiched layer of high temperature is not geologically likely which seems to rule out elevated temperatures. Another possibility is secondary mineralization filling the pore space of Honomanu basalt. This does not seem unreasonable since S15 is

located on the dormant north rift zone of Haleakala. Perhaps an old geothermal field existed at this location at one time, causing hydrothermal alteration products to be deposited in the pore space of the surrounding basalt. Zeolites, a common alteration product in Hawaii, could cause a basalt layer containing freshwater to become more conductive (Birch, 1942).

15. SOUNDING 17

Sounding 17 (S17) was located at 110 meters elevation near the north rift zone of Haleakala. The sounding was oriented normal to the coast line. The field curve is best modeled with 6 layers. The first 3 layers are relatively thin and difficult to resolve. High correlation between the resistivity parameters of the first 3 layers imply large errors for these 3 resistivities. The best-fit curve is achieved by fixing the 5th layer resistivity to 495 ohm-m. The coastal correction improves the model fit without changing any model parameters. This is the only sounding where this occurred.

The basement resistivity is 22.5 ± 13 ohm-m and is interpreted as seawater-saturated basalt. The calculated porosity is 12% and the calculated head is 1.8 meters. The field curve, best-fit model, and geologic interpretation are given in Figure 25. Nearby well-logs show heads averaging around 1.5 meters in Honomanu basalt.

16. SOUNDING 18

Sounding 18 (S18) was located east of Paia town at 91.4 meters elevation on a sugar cane road. S18 was located 3.2 kilometers from

Parameter Correlation Matrix

ρ_1	ρ_2	ρ_3	ρ_4	ρ_5	ρ_6	t_1	t_2	t_3	t_4	t_5	
1.0	.99	.94	.29	.12	.10	-1.0	1.0	-.94	.15	.12	ρ_1
	1.0	.95	.31	.13	.11	-1.0	1.0	-.95	.16	.13	ρ_2
		1.0	.56	.27	.22	-.95	.95	-1.0	.31	.27	ρ_3
			1.0	.66	.54	-.31	.32	-.56	.70	-.66	ρ_4
				1.0	.94	-.13	.13	-.26	1.0	-1.0	ρ_5
					1.0	-.10	.11	-.21	.93	-.94	ρ_6
						1.0	-.10	.95	-.16	.13	t_1
							1.0	-.95	.16	-.14	t_2
								1.0	-.31	-1.0	t_3
									1.0	-1.0	t_4
										1.0	t_5

ρ_a (ohm-meters)

$\rho_1 = 1512$
$T_1 = 1.1$

$\rho_3 = 2410$
$T_3 = 1.7$

Sea Level

$\rho_2 = 82$
$T_2 = 1.2 \pm 2$

$\rho_4 = 134 \pm 20$
$T_4 = 69 \pm 17$

$\rho_5 = 495$
$T_5 = 109 \pm 17$

$\rho_6 = 22.5 \pm 13$

Best Fit Model
S = 5.1%

Soil

Fresh Water
(Kula or Weathered Honomanu)
Basalt

Sea Water Basalt
(Honomanu)

Geologic Interpretation

Road Fill

Kula Basalt
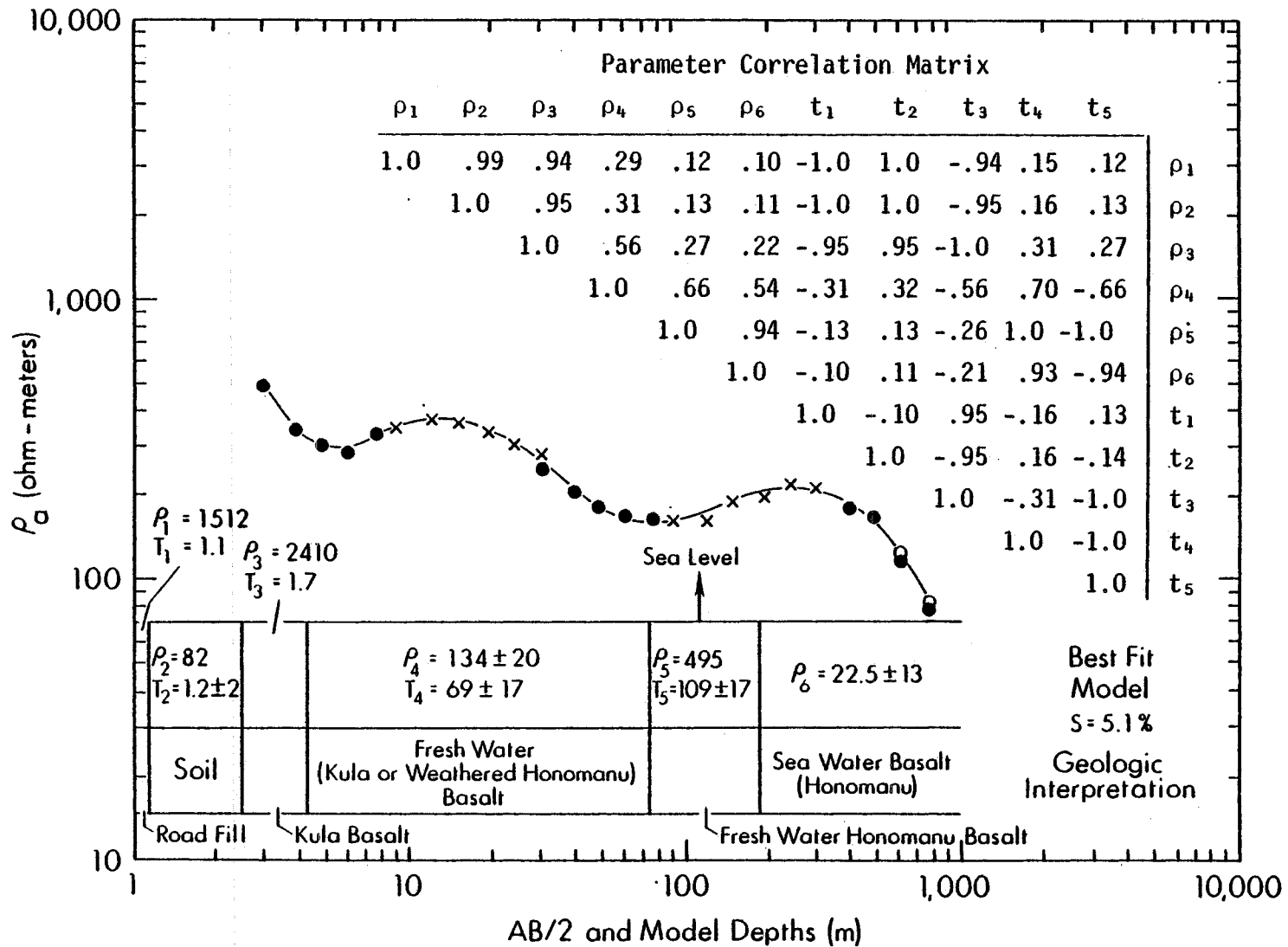
Fresh Water Honomanu Basalt

AB/2 and Model Depths (m)

Figure 25. S17 apparent resistivity curve, best fit model and geolgic interpretation. Model parameters are unaffected by the coastal correction.
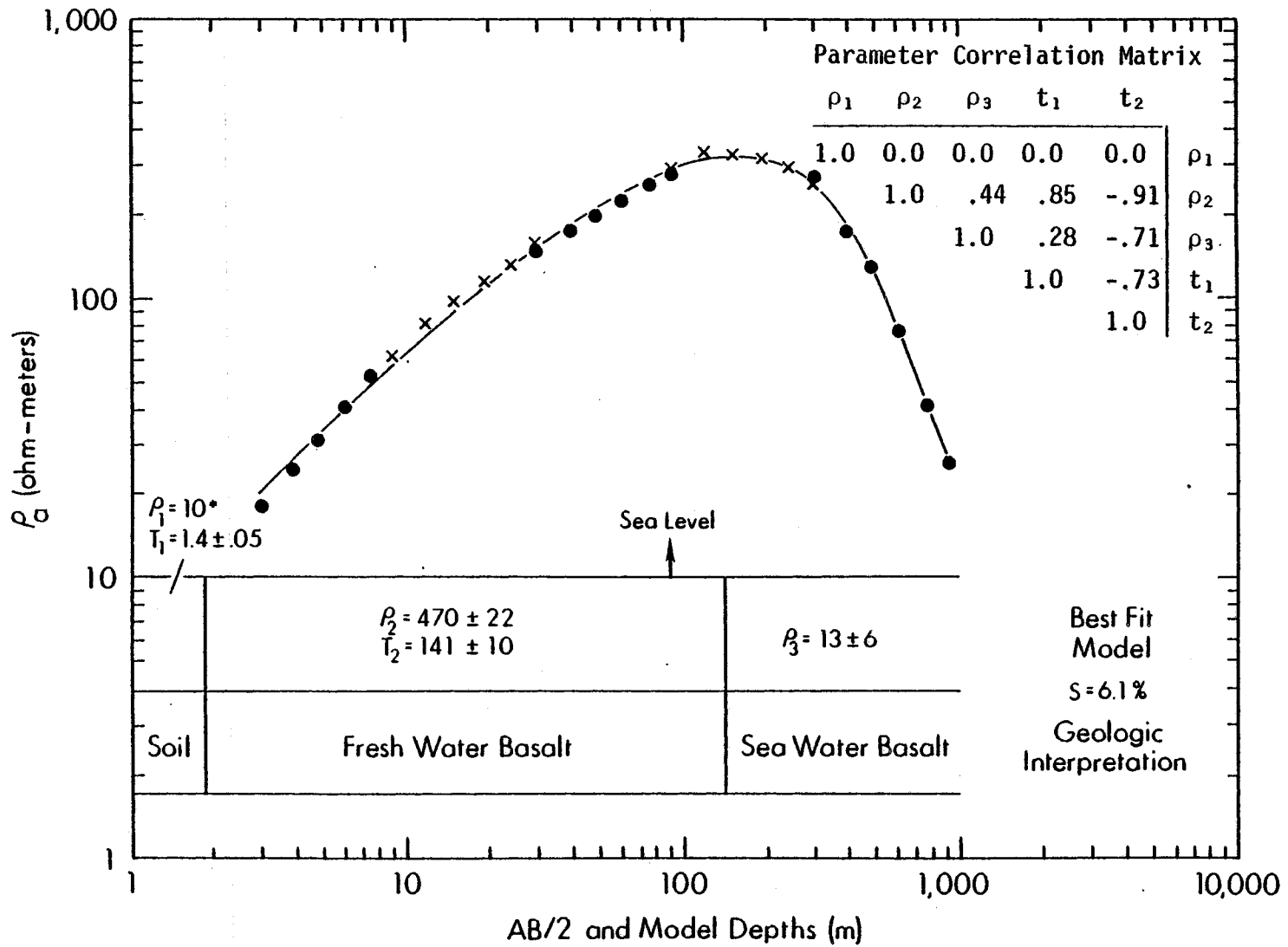
Figure 26.   S18 apparent resistivity curve, best fit model and geologic interpretation.

the coast; no coastal correction was necessary. The field curve was inverted to 3- and 4-layered models with the 3-layered models giving the best fit. Well 28 is situated at 90 meters elevation in the town of Paia. The reported head of well 28 is 1.2 meters and Honomanu basalt is the aquifer. Water temperature is 21°C.

The resistivity of the basement in S18 is 13 ± 6 ohm-m. This corresponds to 18% porosity for 20°C seawater-saturated basalt. The calculated head is 1.3 meters, in excellent agreemnent with well 28.

Nearby wells 25, 27 and 28 show Kula basalt to be between 15 and 38 meters thick in the surrounding area. In general, the well logs show Kula basalt to be more massive and Honomanu basalt to be more porous. S18 does not show an electrical distinction between freshwater-bearing Kula and Honomanu basalt, as S15 and S17 do. Since a 4-layered model does not fit the data the results imply that the porosity for Kula and Honomanu basalt are the same (18%) at this location.

17. SOUNDING 19

Sounding 19 (S19) was located on the trace of Haleakala's north rift zone, north of Haiku town. S19 was oriented parallel to and 975 meters from the coast. The elevation is 29 meters. The sounding was inverted to 3- and 4-layered models with the 4-layered model providing the best fit.

The coastal correction increases the basement resistivity 13%, from 7.8 to 9.0 ohm-m. A correlation coefficient of -1.0 between ρ_3 and t_3 imply poor resolution for these two parameters. The thickness of the thin first layer is difficult to resolve because data were not

Parameter Correlation Matrix

ρ_1	ρ_2	ρ_3	ρ_4	t_1	t_2	t_3	
1.0	-.64	-.09	.02	0.0	-.12	.09	ρ_1
	1.0	.16	-.04	0.0	.21	-.16	ρ_2
		1.0	.34	0.0	.99	-1.0	ρ_3
			1.0	0.0	.31	-.34	ρ_4
				1.0	0.0	0.0	t_1
					1.0	-.99	t_2
						1.0	t_3

$\rho_1 = 31 \pm 3$
$T_1 = 0.6^*$

Sea Level

$\rho_3 = 500$
$T_3 = 10$

$\rho_2 = 44 \pm 0.5$
$T_2 = 42 \pm 1.5$

$\rho_4 = 9.0 \pm 0.6$
(7.8)

Coastal Corrected Model
(Uncorrected Model)

S = 4.1%

Fresh Water Soil
and Kula Basalt Mixture

Sea Water
Honomanu Basalt

Geologic Interpretation

Soil

Fresh Water
Honomanu Basalt
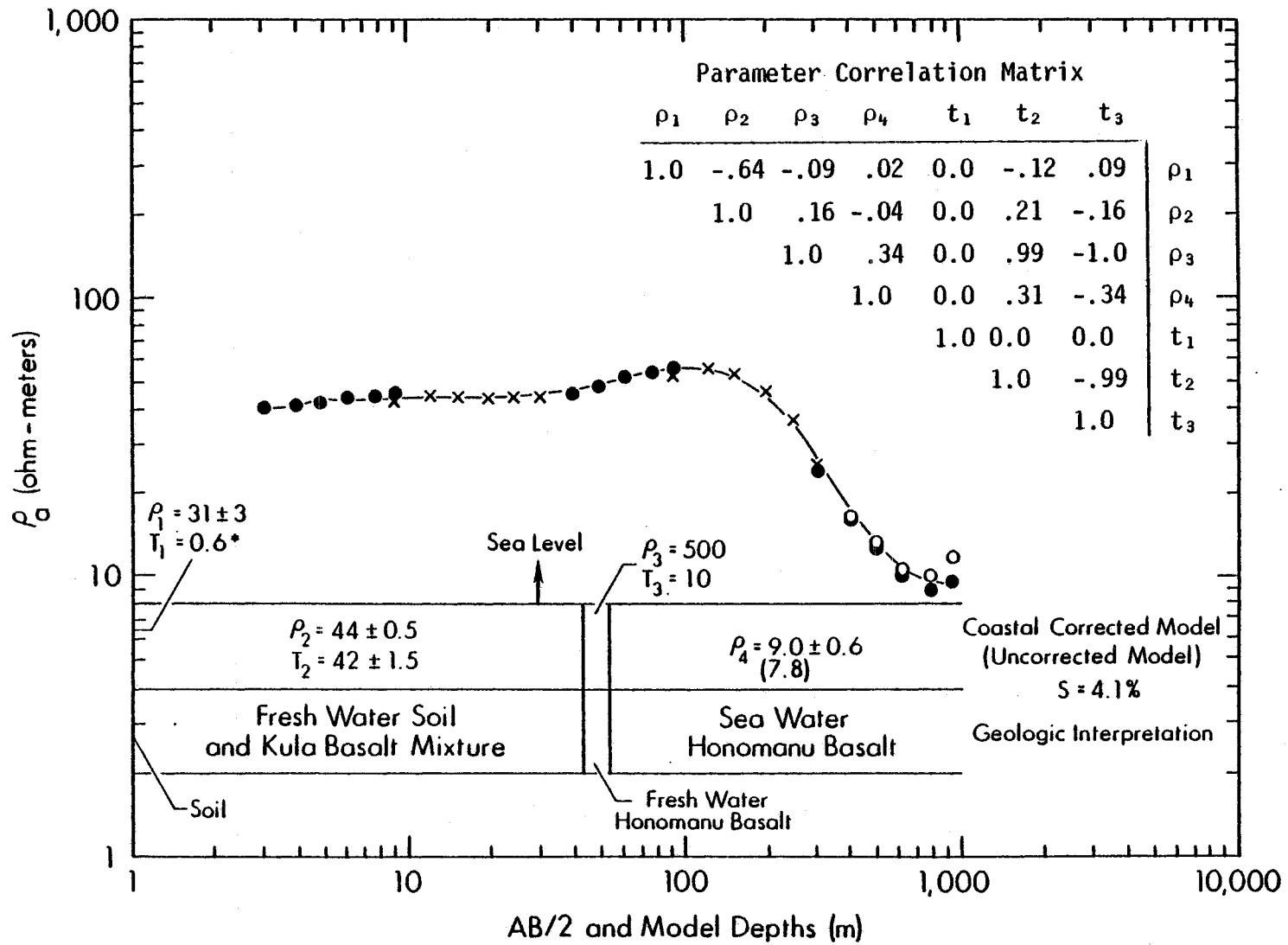
ρ_a (ohm - meters)

AB/2 and Model Depths (m)

Figure 27. S19 apparent resitivity curve, best fit model and geologic interpretation.

taken at AB/2 less than 3 meters. The rest of the parameters in S19 are well resolved.

Comparison of S19 with logs from well 32, 2.9 km to the west, gives the following interpretation. The first layer is soil, the second layer is a mixture of ash and thin Kula basalt flows, the third and fourth layers are freshwater then seawater-saturated Honomanu basalt.

The calculated porosity is 24% for 20°C, seawater-saturated basalt. The calculated head is 0.6 meters. Similar interpretations were given by S18 and S17 located on either side of S19. Figure 27 shows the geologic interpretation in bar form.

18. SOUNDING 20

Sounding 20 (S20) was located in Keanae valley at 99 meters elevation. S20 was oriented normal to and 1524 meters from the coast. The coastal correction has no effect on the interpretation of S20. A wire link fence runs parallel to S20 and is intermittantly anchored with metal posts. Starting at AB/2 = 40m, erratic behavior of some points is probably caused by intermittent shorting by the fence. The data are good enough, however, to yield the resisitivity of the basement, which is our target.

The field curve is best modeled by a 5-layered curve. The fourth layer parameters are perfectly correlated (-1.0), therefore only the transverse resistance ($\rho_4 \cdot t_4$) can be uniquely resolved. By the principle of equivalence (Keller and Frischknecht, 1966) a minimum resistivity of 498 ohm-m and a miximum thickness of 63.4 meters can be assigned to the fourth layer. If we interpret the basement interface as the boundary
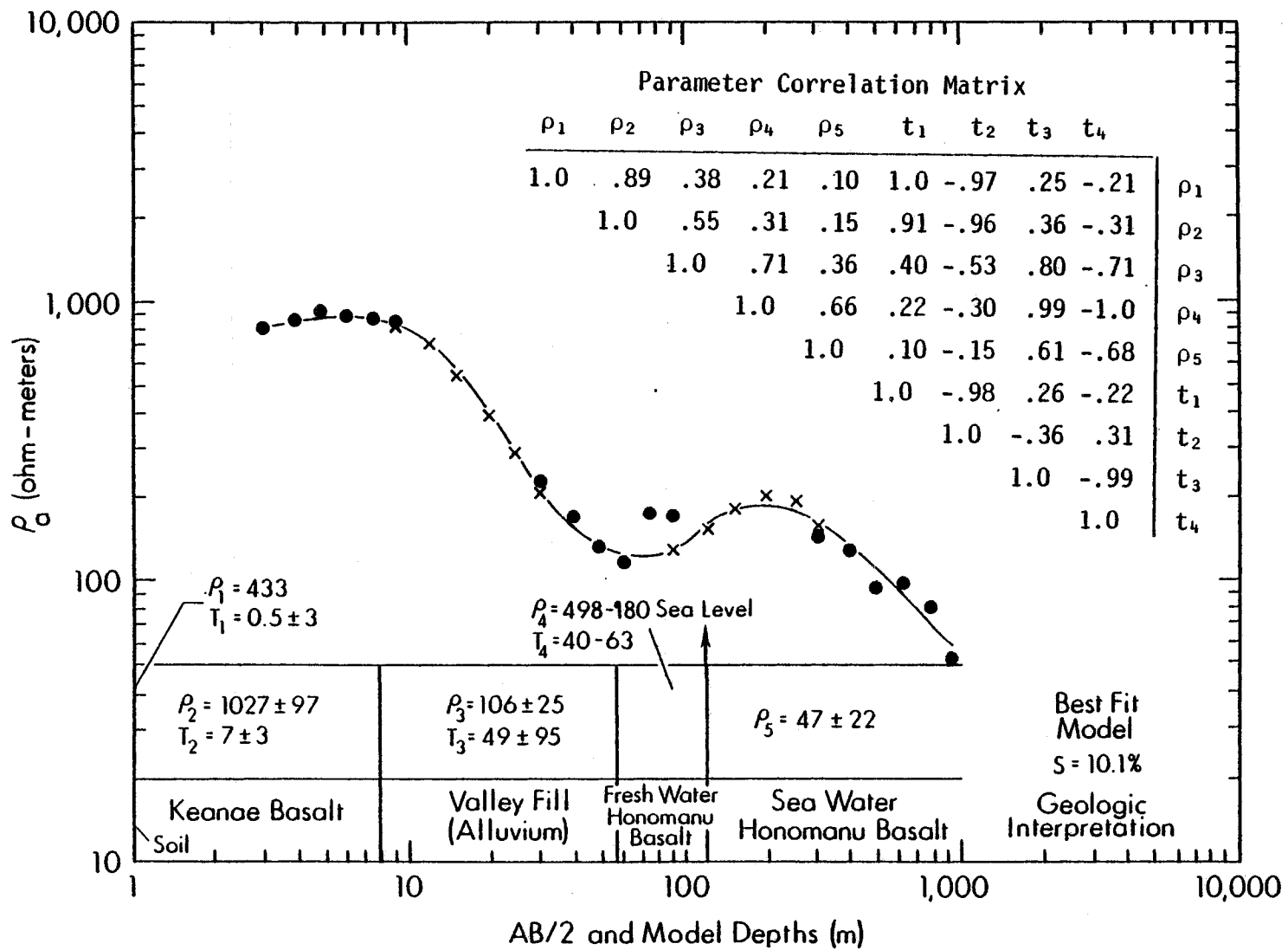
Figure 28. S20 apparent resistivity curve, best fit model and geologic interpretation.

between seawater and freshwater then we can assign a minimum thickness to the fourth layer by making the basement correspond to sea level. This is geologically reasonable since seawater is unlikely to occur above sea level. By using these constraints we find the fourth layer resistivity to range from 780 to 498 ohm-m and the thickness to range from 40 to 63.4 meters.

Comparison of S20 and the geology as mapped by Stearns and Macdonald (1942) yields the interpretation shown in Figure 28. The third layer is thick alluvial valley fill which is exposed at the coast. This alluvium perches water which emanates at Ohia and Stone springs located about 1 km east of S20. The low resistivity of the third layer suggest it contains water: perhaps a perched freshwater lens. Well 100 is located 3 km inland of S20; this well penetrates perched water in alluvium at 280 meters above sea level.

The basement is interpreted as seawater-saturated Honomanu basalt with a resistivity of 47 ± 22 ohm-m. This corresponds to a calculated porosity range of 6 to 12%. Thermal waters are not likely for this area. Large quantities of shallow perched water could be developed in this area.

19. SOUNDING 21

Sounding 21 (S21) was located at the mouth of Ukumehame valley 488 meters east of well 12. S21 was oriented parallel to the coast at 24 meters elevation. The field data were inverted to 3-, 4-, and 5-layered models with the 4-layered model giving the best fit.

Parameter Correlation Matrix

	ρ_1	ρ_2	ρ_3	ρ_4	t_1	t_2	t_3	
	1.0	0.0	-.02	-.12	1.0	-.11	.15	ρ_1
		1.0	0.0	0.0	0.0	0.0	0.0	ρ_2
			1.0	.32	-.02	-.93	-.82	ρ_3
				1.0	-.12	-.23	-.60	ρ_4
					1.0	-.11	.15	t_1
						1.0	.67	t_2
							1.0	t_3

$\rho_1 \leq 24$
$T_1 \leq 1.8$

Sea Level

$\rho_2 \geq 300*$
$T_2 \leq 10.8$

$\rho_3 = 58 \pm 9$
$T_3 = 63 \pm 10$

$\rho_4 = 4.3 \pm 1.7$
(3.9)

Coastal Corrected Model
(Uncorrected Model)
S = 5.1 %

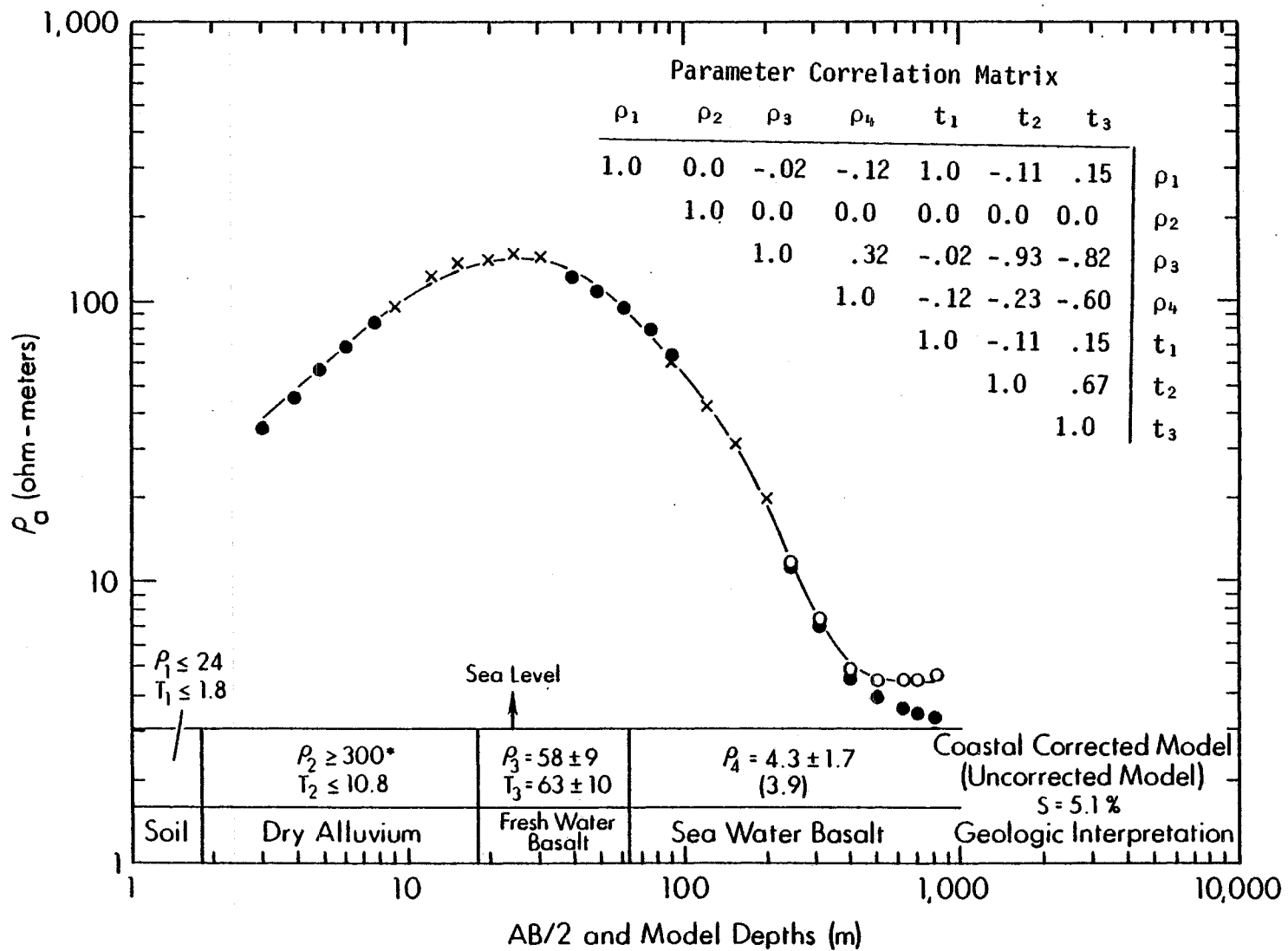| Soil	Dry Alluvium	Fresh Water Basalt	Sea Water Basalt	Geologic Interpretation

Figure 29. S21 apparent resistivity curve, best fit models and geologic interpretation. Note how application of the coastal correction flattens out the end of the curve.

The first 2 layers are plagued with equivalence. The first layer has a horizontal conductance of 13 ohms, a miximum resistivity of 24 ohm-m and a maximum thickness of 1.8 meters. The second layer has a transverse resistance of 3240 ohm-m^2, a minimum resistivity of 300 ohm-m and a maximum thickness of 10.8 meters.

The bottom 2 layers are well resolved. The basement resistivity was increased from 3.9 to 4.2 ohm-m by the coastal correction. This low resistivity basement is also seen in S12 and S8, which are located near Ukumehame. The basement is interpreted as warm, seawater-saturated Wailuku basalt. The third layer also has a low resistivity of 58 ± 9 ohm-m and is interpreted as warm, freshwater-bearing basalt. The calculated head is 1.25 meters, in excellent agreement with well 12 with a measured head of 1.0 to 2.0 meters.

IX. SUMMARY

In 1965--6, 32 Schlumberger soundings were performed near Waialua, Oahu, by Zohdy and Jackson (1969). Their interpretation yielded the following classification:

Table 2

Resistivities of Various Rock Types Measured Near Waialua, Oahu

Rock Type	Resistivity (ohm-meters)
Clay saturated with brackish to saline water	< 3
Clay saturated with brackish to fresh water	5 - 8
Clay, silt, sand, gravel saturated with freshwater	11 - 25
Sand and coral	40 - 400
Weathered basalt saturated with freshwater	30 - 60
Fresh basalt saturated with freshwater	300 - 700
Fresh basalt saturated with saline water	30 - 40

In 1967, 14 Schlumberger soundings were performed near Pahala, Hawaii as part of a Master of Science thesis by Donald Hussong (1967). His results were roughly categorized as follows:

Table 3

Resistivities of Various Rock Types Measured Near Pahala, Hawaii

Rock Type	Resistivity (ohm-meters)
Unweathered Aa lava	10,000 - 200,000
Unweathered Pahoehoe Lava	5,000 - 20,000
Weathered lavas	1,000 - 8,000
Dry soil	500 - 5,000
Wet soil	50 - 500
Freshwater-saturated lavas	50 - 300

The range of resistivities interpreted from 19 Schlumberger soundings performed on Maui and reported in this thesis, yield the following classification as shown in Table 4.

These results show that the D.C. resistivity method is a useful technique for geothermal and groundwater exploration in Hawaii. The large contrast between basalt saturated with freshwater and seawater provides a useful signature to delineate subsurface water characteristics.

Table 4

Resistivities of Various Rock Types Measured on Maui

Rock Type	Resistivity (ohm-meters)
Dry soil	170 - 800
Wet soil	10 - 100
Dry alluvium	150 - 300
Wet alluvium	50 - 150
Dry basalt	2,000 - 20,000
Freshwater-bearing basalt	300 - 900
Weathered freshwater-bearing basalt	45 - 150
Seawater-saturated basalt	10 - 60
Warm freshwater basalt	25 - 60
Warm seawater-saturated basalt	3 - 8

X. DISCUSSION AND CONCLUSIONS

Interpretation of Schlumberger apparent resistivity data seldom uniquely resolves all the layers encountered in a typical geologic column. The effects of anisotropy and local heterogeneities often distort the data. Even when the assumption of isotropic and homogeneous horizontal layers has not been violated, interpretation problems sometimes exists as a consequence of the principles of equivalence and suppression. Many of the problems can be minimized using geologic constraints from nearby well logs. The most problematic layers, in this study, were thin shallow layers. Unfortunately the errors produced by these thin shallow layers sometimes propagate, confusing the interpretation of the deeper thicker layers.

The strength of the Schlumberger method is the ability to resolve the resistivity of a conductive basement. This parameter is often well resolved because of good current penetration as the current seeks out the conductor; also the field curve asymptotically approached the resistivity of the basement, even in the presence of local heterogeneities or anisotropic surface layers. The thick seawater-saturated basalt unit which underlies Maui island provides such a conductive layer. However, if the seawater basement is too deep it is often impossible to attain the electrode separation neccessary to determine its electrical properties. Comparison of resistivity values for seawater-saturated basalt across the island of Maui may indicate areas of anomolous subsurface heat.

Of the twenty-one soundings performed on Maui, fourteen resolve the resistivity of the seawater-saturated basalt basement. Two were affected

Table 5

Resistivity of Maui Basalt Containing Seawater or Freshwater

Location	Sounding Number	Resistivity Freshwater Basalt (Ω-m)	Resistivity Seawater Basalt (Ω-m)
Launiupoko	S1	375	58
Lahaina	S2	375	24
Lahaina	S6	595*	--
Lahaina	S7	600	38
Honolua	S10	420*	37
Honolua	S11	--	<60
Olowalu	S5	97	7.7
Ukumehame	S8	26	3.9
Ukumehame	S12	30	4.3
Ukumehame	S21	58	4.3
Maalaea	S9	350 - 750	13.4
Paia	S15	302† 65√	10.5
Paia	S17	134† 495*√	22.5
Paia	S18	470	13.0
Paia	S19	85	9.8
Keanae	S20	498 - 780	47.0
Hana	S14	400	<50
Haleakala South Rift	S13	856	--

†Kula basalt   √Honomanu basalt
*parameters which were held fixed during the inversion

by water pipes, two did not penetrate the seawater basement and two had insufficient spread length to resolve the basement resistivity. Table 5 tabulates the resistivities of seawater-saturated and freshwater-bearing basalt encountered on Maui. The most conductive region encountered is at Ukumehame canyon on West Maui.

Depth to the seawater basement is sometimes difficult to resolve. If the thickness of any layer above the basement cannot be accurately estimated, due to high correlation with other layers or anisotropy, then the depth to the seawater basement may also be inaccurate. In some cases it is not clear how many layers are represented by the field curve. Different number of layers may give different depths to the seawater basement. Occasionally the addition of a layer slightly improves the goodness of fit. In these cases it becomes important to compare nearby well log data. Even in the most severe cases of equivalence some additional subsurface information can usually be gained by comparison of results with nearby well or sounding data.

Table 6 tabulated the piezometric head calculated from the Schlumberger data and compares the observed head values from nearby wells (see Figure 1 for locations). In general the Schlumberger data are in excellent agreement with the well observations. The largest freshwater head encountered on Maui is in Keanae Valley (91.2 meters). This large volume of water is perched on the Keanae valley fill as observed in well 100. All other heads are under 4 meters, showing a rather thin freshwater lens near the coastline at the areas surveyed.

Table 6

Comparison of Piezometric Heads Observed in Nearby Wells to
the Heads Computed Using the Resistivity Data

| Location	Well or Sounding Number	Elevation (meters)	Head (meters)
Lahaina	W292	134.7	.46-.88
	S7	114.3	.67
	S2	79.2	1.0
	W1	78.3	.82
	W318	273.4	1.77-2.07
	S10	170.7	1.73
Olowalu	S5	61.0	1.77
	W10	50.3	1.07
Ukumehame	W12	24.1	1.04-2.04
	S12	44.2	3.63
	S8	22.9	1.65
	S21	24.0	1.25
Maalaea	S9	19.8	0.03-0.91
	W110	100.9	1.98
	W14	7.9	1.22
	W15	91.4	0.98
Paia	W22	63.1	1.5
	S18	91.4	1.3
	W28	89.9	1.2
	S19	29.0	1.8
	W31	47.5	1.3
	S15	99.1	2.7
	W32	109.7	1.2
	S17	109.7	1.8
Keanae	S20	99.1	91.2
	W100	378.0	281.0
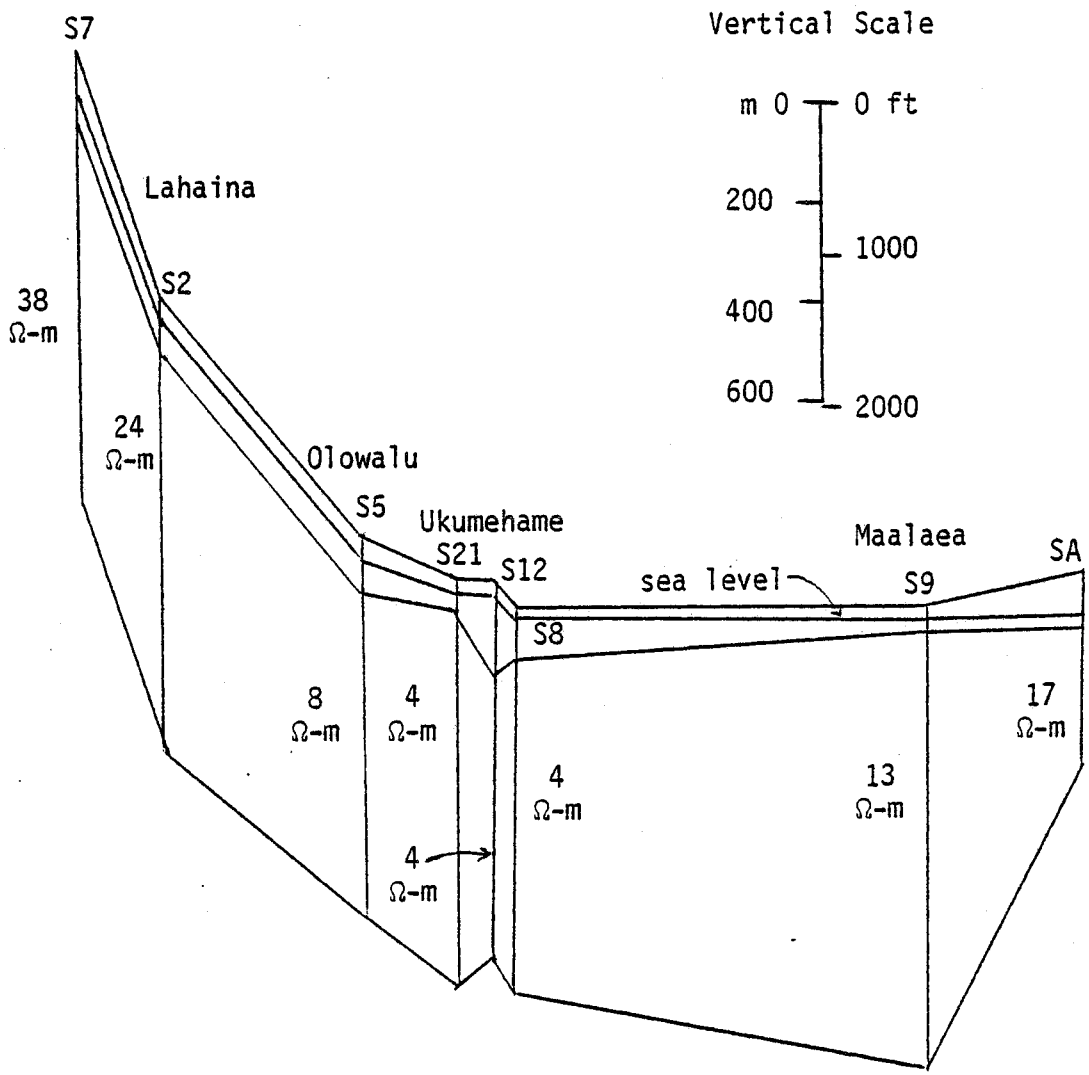
Figure 30. Cross-section of basement resistivities and freshwater lens around the southern coast of West Maui (see Fig. 1). The lowest resistivities are found near Ukumehame valley. All values are interpreted to be seawater-saturated basalt. Vertical exaggeration is 5:1.
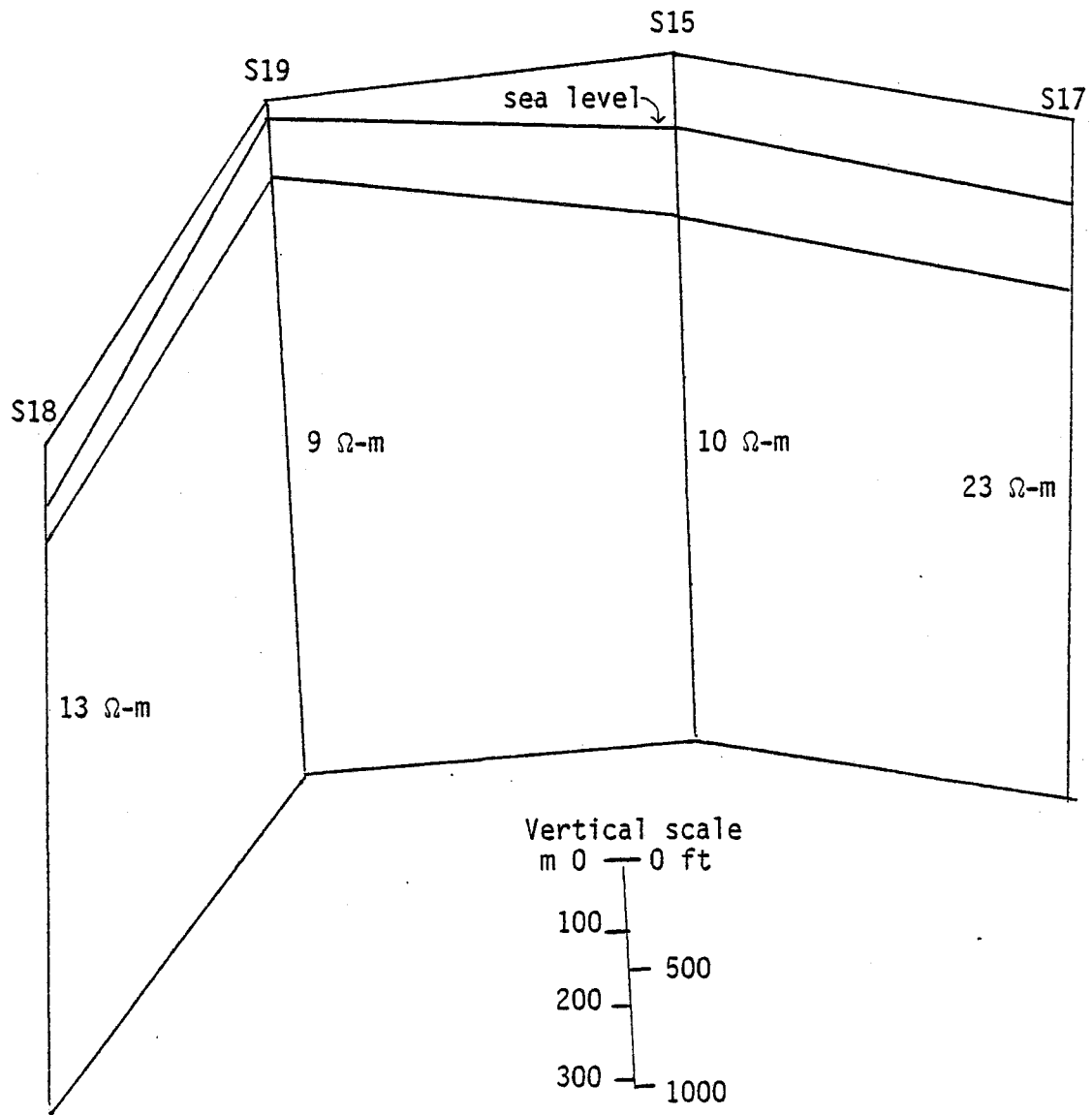
Figure 31. Cross-section of basement resistivities and freshwater lens across the north rift zone of Haleakala. The lowest values correspond with the trace of the rift zone (for locations see Fig. 1). Vertical exaggeration is 10:1.

A cross-section of basement resistivities, with the calculated freshwater lens, across West Maui's south rift zone is presented in Figure 30. Note the relatively low values of basement resistivity in Ukumehame valley.

A cross-section of basement resistivities, with the calculated freshwater lens, across the north rift zone of Haleakala is shown in Figure 31 (for location see Figure 1). The lowest resistivities correspond with the trace of the rift zone.

In conclusion, the most promising area for geothermal development, interpreted from the resistivity data, is Ukumehame canyon. A cross section of the Ukumehame area showing local geology, without vertical exaggeration, is presented in Figure 32. Using equation (11) and typical porosities for Hawaiian basalt, the following temperatures are calculated.

Table 7

Temperatures Calculated Near Ukumehame Canyon

Porosity (%)	T°C*	T°C†
10	289	322
15	153	171
20	95	107
25	62	71
30	43	50

*uses the mean seawater-saturated basalt resistivity interpreted from the coastal corrected models (4.1Ω-m)

†uses the mean uncorrected seawater-saturated basalt resistivity (3.7Ω-m) from soundings S8, S12, and S21

REFERENCES CITED

Adams, W.M., 1968. Evaluation of Some Geophysical Techniques Applied to the Environment of a Maui Well. Hawaii Inst. Geophys. Rept., HIG-68-23, 29 p.

Andersen, W.L., 1975. Improved Digital Filters for Evaluating Fourier and Hankel Transform Integrals. U.S.G.S. Report USGS-GD-75-012, 223 p. available from U.S. Dept. of Commerce, National Info. Service (NTIS), Springfield, VA 22161 as Report PB-242-800/IWC.

Anderson, W.L., 1979. Program MarqDclag: Marquardt Inversion of DC-Schlumberger Soundings by Lagged-Convolution. U.S. Geol. Survey Open File Rept. 79-1432, 58 p.

Bevington, P.R., 1969. Data Reduction and Error Analysis for the Physical Sciences. McGraw-Hill Book Co., p. 56-60.

Birch, F., 1942. Handbook of Physical Constants, edited by Francis Birch. Geol. Soc. of America Sp. Papers, No. 36, p. 308-312.

Compagnie Generale de Geophysique, 1955. Abaques de Sondage Electrique. Geophys. Prospect., v. 3, suppl. no. 3.

Cox, A., 1969. Geomagnetic Reversals. Science, v. 163, p. 237-45.

Darknov, V.N., 1962. Geophysical Well Logging. Q. Colo. Sch. of Mines, v. 57, no. 2.

Draper, N.R. and H. Smith, 1966. Applied Regression Analysis. John Wiley and Sons, Inc., p. 64-67.

Evjen, H.M., 1938. Depth Factors and Resolving Power of Electrical Measurements. Geophysics, v. 3, p. 78-95.

Ghosh, D.P., 1971. The Application of Linear Filter Theory to the Direct Interpretation of Geoelectrical Resistivity Sounding Measurements. Geophys. Prospect., v. 19, p. 192-217.

Hussong, D.M., 1967. A Study of Ground Water Configuration Near Pahala, Hawaii by the D.C. Electrical Resistivity Method. Mast. Thesis, Univ. of Hawaii, 88 p.

Inman, R.J., 1975. Resistivity Inversion with Ridge Regression. Geophys., v. 40, p. 798-817.

Jenkins, M.G. and D.G. Watts, 1968. Spectral Analysis and Its Applications. Holden-Day, 525 p.

Keller, G.V. and F.C. Frischknecht, 1966. Electrical Methods in Geophysical Prospecting. Pergamon Press, New York, 517 p.

King, L.V., 1934. On the Flow of Electric Current in Semi-Infinite Media in Which the Specific Resistance is a Function of Depth. Royal Soc. London Philos. Trans., Ser. A, v. 233, p. 327-359.

Kinoshita, W.T. and R.T. Okamura, 1965. A Gravity Survey of the Island of Maui, Hawaii. Pacific Science, v. 19, no. 3, p. 339.

Koefoed, O., 1972. A Note on the Linear Filter Method of Interpreting Resistivity Sounding Data. Geophys. Prospect., v. 20, p. 403-405.

Koefed, O., 1979. Geosounding Principles, 1; Resistivity Sounding Measurements. Elsevier Scientific Publishing Co., 276 p.

Kunetz, G., 1966. Principles of Direct Current Resistivity Prospecting. Borntraeger, Berlin, 101 p.

Macdonald, G.A. and A.T. Abbott, 1970. Volcanoes in the Sea. University of Hawaii Press, Honolulu, 441 p.

Maillet, R., 1947. The Fundamental Equations of Electrical Prospecting. Geophysics, v. 12, p. 529-556.

Malahoff, A. and G.P. Woollard, 1965. Magnetic Surveys over the Hawaiian Ridge. Hawaii Inst. Geophys. Tech. Rept., HIG-65-11, 64 p.

Marquardt, D.W., 1963. An Algorithm for Least-Squares Estimation of Nonlinear Parameters. Jour. Soc. Indust. Appl. Math, v. 11, no. 2, p. 431-441.

Mundry, E., 1980. The Effect of a Finite Distance Between Potential Electrodes on Schlumberger Resistivity Measurements - A Simple Correction Graph. Geophysics, v. 45, no. 12, p. 1872-1875.

Mundry, E. and P. Worzyk, 1979. On the Coastal Effect on Geoelectric Soundings. Journal of Geophysics, v. 45, p. 329-336.

Olhoeft, G.R., 1977. Electrical Properties of Water Saturated Basalt Preliminary Results to 506K (233°C). U.S.G.S. Open File Rept. D-77-785, 6 p.

Pekeris, C.L., 1940. Direct Method of Interpretation in Resistivity Prospecting. Geophysics, v. 5, p. 31-42.

Peterson, F.L. and M.M. Segal, 1974. Determining Porosity with Neutron Logs from Hawaiian Basalt Aquifers. Water Resour. Res. Center Tech. Rept., no. 80, 37 p.

Rai, S.R., 1977. Electrical and Elastic Properties of Basalts and Ultramafic Rocks as a Function of Saturation Pressure and Temperature. PhD Dissertation, Univ. of Hawaii, 155 p.

Roy, A. and A. Apparao, 1971. Depth of Investigation in Direct Current Methods. Geophysics, v. 36, no. 5, p. 943-959.

Slichter, L.B., 1933. The Interpretation of the Resistivity Prospecting Method for Horizontal Structures. Physics, v. 4, p. 307-322.

Stearns, H.T. and G.A. Macdonald, 1942. Geology and Ground-Water Resources of the Island of Maui, Hawaii. Hawaii Div. Hydrog. Bull., no. 7, 344 p.

Stefanesco, S.S., C. Schlumberger, and M. Schlumberger, 1930. Sur la Distribution Electrique Potentielle Autour D'une Prise de Terre Ponctuelle Dans un Terrain a Couches Horizontales Homogenes et Isotropes. Jour. Physique et Radium, ser. 7, v. 1, p. 132-141.

Swartz, J.H., 1937. Resistivity Studies of Some Salt Water Boundaries in the Hawaiian Islands, Trans. A.G.U., v. 18, p. 387-393.

Swartz, J.H., 1940. Geophysical Investigations in the Hawaiian Islands. Trans. A.G.U., v. 20, p. 292-298.

Thomas, D., M. Cox, D. Erlandson, and L. Kajiwara, 1979. Potential Geothermal Resources in Hawaii: A Preliminary Regional Survey. Hawaii Inst. Geophys. Tech. Rept., HIG-79-4, 103 p.

U.S. Geological Survey, 1980. Well Logs and Data on File. Honolulu Office, Honolulu.

Zohdy, A.A., G.P. Eaton and D.R. Mabey, 1974. Application of Surface Geophysics to Ground-Water Investigations. In Tech. Water-Resources Inves.: U.S.G.S., Book 2, Chap. D1, p. 41.

Zohdy, A.A.R. and D.B. Jackson, 1969. Application of Deep Electrical Soundings for Groundwater Exploration in Hawaii. Geophysics, v. 40, no. 4, p. 584-600.